International Journal of Thermal Sciences 163 (2021) 106814

Contents lists available at ScienceDirect

International Journal of Thermal Sciences

journal homepage: http://www.elsevier.com/locate/ijts

Investigation of pool boiling heat transfer on hydrophilic-hydrophobic mixed surface with micro-pillars using LBM

Yuan Feng [a], Fucheng Chang [a], Zitu Hu [a], Huixiong Li [a,*], Jianfu Zhao [b,c]

[a] State Key Laboratory of Multiphase Flow in Power Engineering, Xi'an Jiaotong University, Xi'an, 710049, China
[b] CAS Key Laboratory of Microgravity, Institute of Mechanics, Chinese Academy of Sciences, Beijing, 100190, China
[c] School of Engineering Science, University of Chinese Academy of Sciences, Beijing, 100049, China

ARTICLE INFO

Keywords:
Boiling heat transfer
Surface modification technology
Lattice Boltzmann method

ABSTRACT

Surface modification technology by controlling the surface wettability or applying micro/nano-structures to enhance the boiling heat transfer performance has attracted a great deal of interest in recent years. Abundant experiments were performed to investigate the boiling processes on the modified surfaces, and lots of experimental data as well as reliable conclusions were obtained. With the advantages of saving costs and time, the numerical method has been a new reliable way to investigate the bubble dynamics and heat transfer during pool boiling processes on the modified heated surfaces. Pseudopotential LB model is capable of simulating the entire boiling processes including the bubble nucleation, and this model has been successfully applied to simulate the pool boiling processes on both the smooth surfaces and the hydrophilic-hydrophobic mixed surfaces with micro-pillars. However, the numerical simulations of the boiling processes on the mixed surfaces were still rare, and the influence of geometrical parameters of pillar structures of the mixed surface on boiling heat transfer performance was still unclear yet. Moreover, some of the conclusions in existing literature were inconsistent with those in others. Thus it's necessary to carry out more numerical and experimental researches to solve these problems. In this study, the MRT pseudopotential model coupled with phase-change model was applied to simulate the pool boiling processes on the hydrophilic-hydrophobic mixed surface textured with micro-pillars. Under different wall superheats, the bubble dynamics and heat transfer during boiling processes on the mixed surface with micro-pillars were compared to those on the smooth hydrophilic surface and the hydrophilic-hydrophobic mixed surface without micro-pillars. The heat transfer enhancement mechanism of the mixed surfaces was revealed and the influence of geometrical parameters of pillars, including pillar width and pillar number, on bubble dynamics and heat transfer performance during pool boiling processes was investigated in detail.

1. Introduction

As one of the most efficient modes of heat transfer, pool boiling has been widely utilized in numerous industrial devices, such as steam power plants, thermal desalination and electronics cooling systems. However, the heat removal capacity of boiling is limited by the critical heat flux (i.e., CHF) since the heat transfer would be deteriorated when the given heat flux exceeds CHF. To enhance the boiling heat transfer performance and CHF, various technologies could be adopted, such as using external electric fields [1], ultrasonic actuation [2] or magnetic fields [3,4]. Besides, surface modification by controlling the surface wettability or applying micro/nano-scale structures is also an effective technology to enhance pool boiling heat transfer and CHF. Compared with other methods, surface modification technology is easy to process and consumes no extra energy.

Due to these advantages, a great deal of interest has been given to the surface modification technology for pool boiling heat transfer enhancement [5–11]. Using FC-72 as a working medium, Wei and Honda [5] experimentally investigated the pool boiling heat transfer on the heated surfaces with micro-pin-fin structured chips, and they found that the micro-pin-finned chips could cause a considerable enhancement in heat transfer performance in the nucleate boiling region and enhance the CHF. Betz et al. [6] performed experiments to study the boiling heat transfer performance on flat surfaces with networks combining hydrophilic and hydrophobic regions, and they found that CHF and heat transfer coefficient (i.e., HTC) could be enhanced by 65% and 100% when using the flat surfaces combined with both hydrophilic and

* Corresponding author.
E-mail address: huixiong@mail.xjtu.edu.cn (H. Li).

https://doi.org/10.1016/j.ijthermalsci.2020.106814
Received 13 August 2020; Received in revised form 21 December 2020; Accepted 23 December 2020
Available online 11 January 2021
1290-0729/

Nomenclature

a,b,R,ω	parameters in EOS
c_v	specific heat at constant volume
D	pillar pitch distance
$\mathbf{e}_\alpha$	lattice velocity vector
f_α, $\mathbf{f}$	distribution function for density
$\mathbf{F}$	external force
F_α'	forcing term in the velocity space
$\mathbf{F}_{\text{ads}}$	fluid-solid interaction force
$\mathbf{F}_{\text{g}}$	buoyancy force
$\mathbf{F}_{\text{m}}$	intermolecular interaction force
$\mathbf{g}$	gravitational acceleration
G	interaction strength
G_w	a parameter to tune the contact angle
H	pillar height
h_α	distribution function for temperature
h_{fg}	latent heat of vaporization
Ja	Jacob number
l_0	characteristic length
L_x	width of computational domain
L_y	height of computational domain
$\mathbf{M}$	orthogonal transformation matrix
N	pillar number
p	pressure
p_c	critical pressure
p_{EOS}	prescribed non-ideal equation of state
$\mathbf{P}$	pressure tensor
$s(\mathbf{x})$	switch function
$\mathbf{S}$	forcing term in the moment space
$Q_{loc}(x, t)$	local heat flux on the heated surface
$Q_s(t)$	spatial average heat flux
Q	temporal and spatial average heat flux
t	time
t_0	characteristic time
T	temperature
T_c	critical temperature
T_{sat}	saturation temperature
T_b	temperature of the bottom of heated surface
$\mathbf{u}$	fluid velocity
$\mathbf{v}$	real fluid velocity
v_0	characteristic velocity
W	pillar width
w_α	weighting coefficient
$\mathbf{x}$	position

Greek symbols

θ_b, θ_t	contact angle
Δt	time step
ΔT	wall superheat
ρ	density
σ	parameter to tune the mechanical stability
ψ	pseudopotential
λ	thermal conductivity
μ	dynamic coefficient of viscosity
κ	parameter to tune the surface tension
$\mathbf{\Pi}$	viscous stress tensor
$\mathbf{\Lambda}$	diagonal matrix of relaxation time
γ	surface tension
ν	kinematic coefficient of viscosity
χ	thermal diffusion coefficient
τ	relaxation time

Subscripts and Superscripts

*	dimensionless properties
α	lattice direction
c	critical properties
L, V	liquid, vapor
s	heated surface
x, y	direction
eq	equilibrium properties

hydrophobic regions. Jo et al. [7] experimentally tested the nucleate boiling heat transfer performance on a heterogeneous wettability surface composed of a hydrophilic substrate with hydrophobic dots and studied the influence of the number of hydrophobic dots and the pitch distance between dots on boiling heat transfer. They found that the heated surface could have higher HTC at high heat flux without degrading CHF if the hydrophobic dots on the heated surface are much in number and small in diameter. Suroto et al. [8] studied the effect of hydrophobic-spot periphery length on nucleate pool boiling heat transfer on the TiO_2-coated surface with hydrophobic circle spots, and they found that increasing peripheral length of hydrophobic-spot could enhance the HTC. Kumar et al. [9] investigated the boiling heat transfer on three different types of heterogeneous wettable surfaces and studied the effect of heterogeneous wettability on the bubble dynamics and heat transfer during pool boiling. Kumar et al. [9] observed an appreciable enhancement of 98.5% in the HTC on the hydrophobic polymer printed plain copper sample as compared to the plain copper at a lower heat flux of 15 kW/m^2. In addition, with an increase in heat flux, the percentage enhancement in HTC of all the heterogeneous surfaces as compared to the plain copper is decreased. Zhang et al. [10] manufactured 3D grid structures with the scan line spacing method by selective laser melting (SLM) technique and studied the influence of grid structure on nucleate boiling heat transfer and CHF. They found that CHF increases firstly and then decreases with the increasing grid width and achieved peak value when the grid width is about 1.1 mm. MacNamara et al. [11] fabricated Cu-Diamond composite coatings on the heated surface and studied the influence of coatings on boiling heat transfer, and they found that the HTC could be improved up to 300% and the CHF could be enhanced by 35% by the textured surface.

Although lots of experiments were performed to prove that the surface modification technology is capable of improving HTC and CHF, the enhancement mechanism of the modified surfaces on boiling heat transfer has not been well understood [12]. In addition, experimental method has the disadvantages of high cost and time-consuming, and it's hard to obtain some details in the experiments. Numerical method is a good way to solve these problems. Lattice Boltzmann method (LBM) is a mesoscopic method which can intuitively and easily describe the interaction between the fluids and surrounding environments. Still now, LBM is very successful in the simulations of single-phase flow and multi-phase flow. Several multi-phase LB models have been proposed, and pseudopotential LB model [13] is one of the most popular multi-phase flow LB models. Using this model, different phases of fluids can be directly described by different density values and the interface between different phases of fluids can naturally arise, deform, and migrate and even coalesce or vanish [14]. Pseudopotential LB model has been applied successfully to simulate pool boiling at the smooth heated surface [15–20], and the entire boiling processes, including bubble nucleation, could be simulated by this model.

Li et al. [12] firstly studied the surface modification technology for pool boiling heat transfer enhancement by the pseudopotential LB model. They constructed a hydrophilic-hydrophobic mixed surface textured with micro-pillars, as shown in Fig. 1(a), and simulated the

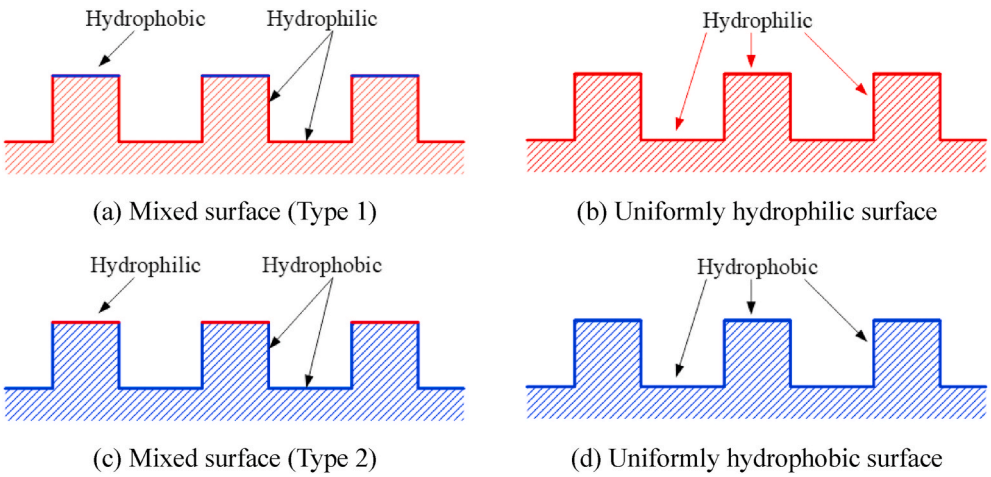

Fig. 1. Four types of heated surfaces textured with pillars used in Ref. [12] or Ref. [21].

pool boiling processes on the mixed surface, and compared the boiling heat transfer performance of the mixed surface to that of a uniformly hydrophilic surface, as shown in Fig. 1(b), and investigated the effect of pillar height, pillar width and the wettability of pillar top on boiling heat transfer performance [12]. They found that the hydrophobicity of the tops of pillars could reduce the wall superheat at ONB, but it also would make the boiling processes enter into the film boiling regime at a lower wall superheat. Ma et al. [21] also simulated the pool boiling processes on the four types of heated surfaces textured with pillars, as shown in Fig. 1(a)~(d), and they found that the heated surface with hydrophobic tops and hydrophilic cavities (i.e., heated surface in Fig. 1(a)) has the highest overall boiling heat transfer performance. In addition, Ma et al. [21] found that the geometrical parameters of pillar structures (including pillar width, pillar height, pillar pitch distance) could greatly affect CHF. More recently, Yu et al. [22] three-dimensionally simulated the pool boiling processes on the hydrophilic-hydrophobic mixed surface and investigated the influence of contact angle of the hydrophilic region, pillar height and pillar width on bubble dynamics and heat transfer during pool boiling processes.

Even though the pool boiling processes on hydrophilic-hydrophobic mixed surfaces textured with pillars have been simulated by Li et al. [12], Ma et al. [21] and Yu et al. [22], there are still some problem needed to be solved. Firstly, the related numerical researches are still rare, and the influence of geometrical parameters of pillar structures on boiling heat transfer has not been fully studied. Concretely, the complete boiling curves of mixed surfaces with different geometrical parameters of pillar structures were not given in Ref. [12] and Ref. [22]. In Ref. [21], when investigating the influence of each geometrical parameter on boiling heat transfer, the boiling curves of only two different mixed surfaces were compared with each other. Secondly, in numerical researches [12,21,22], the boiling heat transfer on the hydrophilic-hydrophobic mixed surface with micro-pillars wasn't directly compared to that on the smooth hydrophilic surface or the hydrophilic-hydrophobic mixed surface without micro-pillars. Thirdly, some numerical results in existing literature are inconsistent with each other. For example, it was found that nucleate boiling heat transfer performance decreases with a decrease in pillar width by Ma et al. [21]. However, in Ref. [12], it seems that an opposite conclusion was obtained. Finally, the number of the pillars is also an important factor that affects the boiling heat transfer performance on the heated surface since the hydrophobic tops and the pillar structures could make a great impact on bubble dynamics under both low and high conditions of wall superheat. However, the influence of pillar number on pool boiling heat transfer on the hydrophilic-hydrophobic mixed surface was rarely considered in the existing numerical researches [12,21,22].

To solve these problems, more related experimental and numerical investigations are needed. In this paper, the MRT pseudopotential LB model coupled with the phase-change model was employed to simulate pool boiling processes on the mixed surfaces textured with micro-pillars consisting of hydrophilic side walls and hydrophobic tops, and these four limitations of previous studies mentioned above were overcome to some extent. To overcome the first and the third limitations, plentiful numerical simulations were carried out to investigate the influence of pillar width on boiling heat transfer under different wall superheats, and the complete boiling curves of different mixed surfaces within a large parameter range of pillar width were obtained. To overcome the second limitation, the boiling heat transfer on the hydrophilic-hydrophobic mixed surface with micro-pillars was directly compared to that on the smooth hydrophilic mixed surface and the hydrophilic-hydrophobic mixed surface without micro-pillars, therefore the mechanism of heat transfer enhancement of the mixed surfaces was revealed. To overcome the fourth limitation, the influence of pillar number on boiling heat transfer performance of the hydrophilic-hydrophobic mixed surface with micro-pillars was investigated in detail. Through observing the evolution of bubble contours, average wetted area fraction, the number of isolated bubbles and spatial average heat flux during the simulations, this study laid a foundation for understanding the influencing mechanism of bubble dynamics on heat transfer during the pool boiling processes on the hydrophilic-hydrophobic mixed surfaces with different geometrical parameters of micro-pillars and designing the pillar structures of mixed surface with the best heat transfer performance.

2. Numerical method

2.1. The MRT pseudopotential LB model

In this study, the pseudopotential LB model with multi-relaxation-time (MRT) collision term was used to solve the distribution of and flow fields. In this model, different phases could be described directly by the densities. The density could be solved by Eq. (1)~(2), which are collision step and streaming step, respectively.

$$f_\alpha^*(\mathbf{x},t) = f_\alpha(\mathbf{x},t) - \left(\mathbf{M}^{-1}\mathbf{\Lambda}\mathbf{M}\right)_{\alpha\beta}\left(f_\beta - f_\beta^{eq}\right) + \Delta t F_\alpha' \tag{1}$$

$$f_\alpha(\mathbf{x}+\mathbf{e}_\alpha\Delta t, t+\Delta t) = f_\alpha^*(\mathbf{x},t) \tag{2}$$

In these equations, f_α is the distribution function of density, and f_α^{eq} is its equilibrium state. $\mathbf{M}$ is an orthogonal transformation matrix. $\mathbf{\Lambda}$ is a diagonal matrix which consists of relaxation times. $\mathbf{e}_\alpha$ is the lattice velocity along the α direction. F_α' is the forcing term in the velocity space. In this study, the exact-difference-method (EDM) forcing scheme was adopted, and F_α' could be expressed as Eq. (3).

$$F_\alpha{}' = w_\alpha \Delta t \left\{ \frac{\mathbf{e}_\alpha \cdot \mathbf{F}}{{c_s}^2} + \frac{[(\mathbf{u} + \ 0.5\Delta\mathbf{u})\mathbf{F} + \mathbf{F}(\mathbf{u} + \ 0.5\Delta\mathbf{u})] : (\mathbf{e}_\alpha\mathbf{e}_\alpha - {c_s}^2\mathbf{I})}{2{c_s}^4} \right\} \quad (3)$$

where ρ is the macroscopic density and $\mathbf{u}$ is the velocity. It should be noted that $\mathbf{u}$ isn't the real fluid velocity. $\Delta\mathbf{u} = \mathbf{F}\Delta t/\rho$, and w_α are the weighting coefficients.

For the D2Q9 model ($\alpha = 0$–8), which is adopted in this study, $\mathbf{e}_\alpha$, $\mathbf{M}$ and $\mathbf{\Lambda}$ can be calculated by Eqs. (4)–(6). The weighting coefficients $w_0 = 4/9$, $w_{1\text{-}4} = 1/9$ and $w_{5\text{-}8} = 1/36$.

$$\mathbf{e}_\alpha = \begin{bmatrix} 0 & 1 & 0 & -1 & 0 & 1 & -1 & -1 & 1 \\ 0 & 0 & 1 & 0 & -1 & 1 & 1 & -1 & -1 \end{bmatrix}^{\mathrm{T}} \quad (4)$$

$$\mathbf{M} = \begin{bmatrix} 1 & 1 & 1 & 1 & 1 & 1 & 1 & 1 & 1 \\ -4 & -1 & -1 & -1 & -1 & 2 & 2 & 2 & 2 \\ 4 & -2 & -2 & -2 & -2 & 1 & 1 & 1 & 1 \\ 0 & 1 & 0 & -1 & 0 & 1 & -1 & -1 & 1 \\ 0 & -2 & 0 & 2 & 0 & 1 & -1 & -1 & 1 \\ 0 & 0 & 1 & 0 & -1 & 1 & 1 & -1 & -1 \\ 0 & 0 & -2 & 0 & 2 & 1 & 1 & -1 & -1 \\ 0 & 1 & -1 & 1 & -1 & 0 & 0 & 0 & 0 \\ 0 & 0 & 0 & 0 & 0 & 1 & -1 & 1 & -1 \end{bmatrix} \quad (5)$$

$$\mathbf{\Lambda} = \mathrm{diag}\left({\tau_\rho}^{-1}, {\tau_e}^{-1}, {\tau_\varsigma}^{-1}, {\tau_j}^{-1}, {\tau_q}^{-1}, {\tau_j}^{-1}, {\tau_q}^{-1}, {\tau_\nu}^{-1}, {\tau_\nu}^{-1}\right) \quad (6)$$

Multiply Eq. (1) with transfer matrix $\mathbf{M}$ and use the method in Ref. [23] to tune the surface tension, the collision step of the LB equations could be rewritten as Eq. (7).

$$\mathbf{m}^* = \mathbf{m} - \mathbf{\Lambda}(\mathbf{m} - \mathbf{m}^{eq}) + \Delta t\mathbf{S} + \mathbf{C} \quad (7)$$

where $\mathbf{m} = \mathbf{M}\mathbf{f}$, $\mathbf{m}^* = \mathbf{M}\mathbf{f}^*$ and $\mathbf{m}^{eq} = \mathbf{M}\mathbf{f}^{eq}$. $\mathbf{m}^{eq}$ could be expressed as Eq. (8). $\mathbf{S}$ is the forcing term in the moment space and can be expressed as Eq. (9). $\mathbf{C}$ is the source term to tune the surface tension and could be calculated by Eq. (10).

$$\mathbf{m}^{eq} = \rho\left(1, -2 + 3\left|\mathbf{u}\right|^2, 1 - 3\left|\mathbf{u}\right|^2, u_x, -u_x, u_y, -u_y, {u_x}^2 - {u_y}^2, u_x u_y\right)^{\mathrm{T}} \quad (8)$$

$$\mathbf{S} = \left(0, 6\mathbf{v}\cdot\mathbf{F} + S_1, -6\mathbf{v}\cdot\mathbf{F} - S_2, F_x, -F_x, F_y, -F_y, 2v_xF_x - v_yF_y, v_xF_y + v_yF_x\right)^{\mathrm{T}} \quad (9)$$

where $S_1 = (\sigma|\mathbf{F}_\mathrm{m}|^2)/(\psi^2\Delta t\tau_e)$, $S_2 = (\sigma|\mathbf{F}_\mathrm{m}|^2)/(\psi^2\Delta t\tau_\varsigma)$.

$$\mathbf{C} = \left[0, \frac{3(Q_{xx} + Q_{yy})}{2\tau_e}, -\frac{3(Q_{xx} + Q_{yy})}{2\tau_\varsigma}, 0, 0, 0, 0, -\frac{Q_{xx} - Q_{yy}}{\tau_\nu}, -\frac{Q_{xy}}{\tau_\nu}\right]^{\mathrm{T}} \quad (10)$$

In Eq. (9), $\mathbf{v}$ is the real fluid velocity and $\mathbf{v} = \mathbf{u} + 0.5\mathbf{F}\Delta t/\rho$. $\mathbf{F}$ is the total external force and $\mathbf{F} = \mathbf{F}_\mathrm{m} + \mathbf{F}_\mathrm{ads} + \mathbf{F}_\mathrm{g}$. $\mathbf{F}_\mathrm{m}$ is the intermolecular interaction force that can be calculated by Eq. (11). $\mathbf{F}_\mathrm{ads}$ is the fluid-solid interaction force that can be expressed by Eq. (12). $\mathbf{F}_\mathrm{g}$ is the buoyancy force that can be calculated by Eq. (13). In Eq. (10), Q_{xx}, Q_{xy} and Q_{yy} could be calculated by Eq. (14).

$$\mathbf{F}_\mathrm{m} = -3G\psi(\mathbf{x})\sum_{\alpha=1}^{8} w_\alpha\psi(\mathbf{x} + \mathbf{e}_\alpha)\mathbf{e}_\alpha \quad (11)$$

$$\mathbf{F}_\mathrm{ads} = -G_w\psi(\mathbf{x})\sum_{\alpha=1}^{8} w_\alpha\psi(\mathbf{x})s(\mathbf{x} + \mathbf{e}_\alpha)\mathbf{e}_\alpha \quad (12)$$

$$\mathbf{F}_\mathrm{g} = (\rho - \rho_{ave})\mathbf{g} \quad (13)$$

$$\mathbf{Q} = 1.5\kappa G\psi(\mathbf{x})\sum_{\alpha=1}^{8} w_\alpha[\psi(\mathbf{x} + \mathbf{e}_\alpha) - \psi(\mathbf{x})]\mathbf{e}_\alpha\mathbf{e}_\alpha \quad (14)$$

In Eq. (11), ψ is the pseudopotential that can be calculated by Eq. (15). G is the intermolecular interaction strength. In Eq. (12), G_w is fluid-solid interaction strength and $s(\mathbf{x} + \mathbf{e}_\alpha)$ is a switch function that is defined as 1 or 0 for solid phase or fluid phase. In Eq. (13), $\mathbf{g}$ is the gravitational acceleration and ρ_{ave} is the averaged density at the computational domain.

$$\psi = \sqrt{\left|\frac{6p_\mathrm{EOS} - 2\rho}{3G}\right|} \quad (15)$$

where p_EOS is the prescribed non-ideal equation of state. In this study, the Peng-Robinson equation of state (P-R EOS) is adopted, as shown in Eq. (16)~(17).

$$p_{EOS} = \frac{\rho RT}{1 - b\rho} - \frac{a\phi(T)\rho^2}{1 + 2b\rho - b^2\rho^2} \quad (16)$$

$$\phi(T) = \left[1 + \left(0.37464 + 1.54226\omega - 0.26992\omega^2\right)\left(1 - \sqrt{T/T_c}\right)\right]^2 \quad (17)$$

where T is the fluid temperature, T_c and p_c are critical temperature and critical pressure, respectively. $a = 0.45724R^2T_c^2/p_c$, $b = 0.0778RT_c/p_c$.

Finally, the macroscopic density ρ and velocity $\mathbf{u}$ could be calculated by Eq. (18).

$$\rho = \sum_\alpha f_\alpha,\ \rho\mathbf{u} = \sum_\alpha \mathbf{e}_\alpha f_\alpha \quad (18)$$

2.2. Liquid-vapor phase-change model

To simulate the liquid-vapor phase-change processes, the energy equation with phase-change source term should be solved. The energy equation used in this study, which is derived from local balance law for entropy, could be expressed as Eq. (19). The detailed derivation of Eq. (19) could be found in Refs. [17,24].

$$\frac{\partial T}{\partial t} + \nabla\cdot(\mathbf{v}T) = \frac{1}{\rho c_v}\nabla\cdot(\lambda\nabla T) + T\left[1 - \frac{1}{\rho c_v}\left(\frac{\partial p_\mathrm{EOS}}{\partial T}\right)_\rho\right]\nabla\cdot\mathbf{v} \quad (19)$$

where λ is the thermal conductivity and c_v is the specific heat. On the right-hand side of Eq. (19), the second term is the phase-change source term. In this study, temperature distribution function, i.e., h_α, is introduced to solve Eq. (19), and the evolution of h_α could be expressed by Eq. (20).

$$h_\alpha(\mathbf{x} + \mathbf{e}_\alpha\Delta t, t + \Delta t) = h_\alpha(\mathbf{x}, t) - \frac{1}{\tau_T}[h_\alpha(\mathbf{x}, t) - {h_\alpha}^{eq}(\mathbf{x}, t)] + w_\alpha\varphi\Delta t \quad (20)$$

where τ_T is the relaxation time for temperature, $\tau_T = \chi/({c_s}^2\Delta t) + 0.5$. χ is the thermal diffusion coefficient. φ is the phase change source term and could be calculated by Eq. (21). h_α^{eq} is the equilibrium distribution function for temperature which given by Eq. (22), and the temperature could be obtained by Eq. (23).

$$\varphi = \frac{1}{\rho c_v}\nabla\cdot(\lambda\nabla T) + T\left[1 - \frac{1}{\rho c_v}\left(\frac{\partial p_\mathrm{EOS}}{\partial T}\right)_\rho\right]\nabla\cdot\mathbf{v} - \nabla\cdot(\chi\nabla T) \quad (21)$$

$${h_\alpha}^{eq} = w_\alpha T\left[1 + \frac{\mathbf{e}_\alpha\cdot\mathbf{v}}{{c_s}^2} + \frac{(\mathbf{e}_\alpha\cdot\mathbf{v})^2}{2{c_s}^4} - \frac{\mathbf{v}^2}{2{c_s}^2}\right] \quad (22)$$

$$T = \sum_\alpha h_\alpha \quad (23)$$

In addition, a conjugate heat transfer problem including heat conduction inside the heated surface is also considered in this study. The method proposed by Li et al. [25] is used to deal with the conjugate heat transfer problem, and the temperature distribution function at the solid-fluid interface could be calculated by Eq. (24)~(25).

$$h_{\alpha^-}(\mathbf{x}_f, t + \Delta t) = \frac{1 - \eta}{1 + \eta}h_\alpha(\mathbf{x}_f, t) + \frac{2\eta}{1 + \eta}h_{\alpha^-}(\mathbf{x}_s, t) \quad (24)$$

$$h_\alpha(\mathbf{x}_s, t + \Delta t) = -\frac{1 - \eta}{1 + \eta}h_{\alpha^-}(\mathbf{x}_s, t) + \frac{2}{1 + \eta}h_\alpha(\mathbf{x}_f, t) \quad (25)$$

where α-is the opposite direction of α, the subscript s and f represent the solid phase and fluid phase, respectively, and $\eta = (\rho c_v)_s/(\rho c_v)_f$.

3. Physical model and computational parameters

The hydrophilic-hydrophobic mixed heated surface adopted in this study is similar to those in Ref. [12] and Ref. [21], and the schematic of the mixed heated surface is shown in Fig. 2(a). As shown, the heated surface is textured with micro-pillars. The bottom substrate and the side walls of pillars are hydrophilic, while the tops of the pillars are hydrophobic. The thickness of the bottom substrate and the height of the pillars are H_0 and H, respectively. The width of the pillars is W, the pillar pitch distance is D, and the number of the pillars is N. In the simulations,

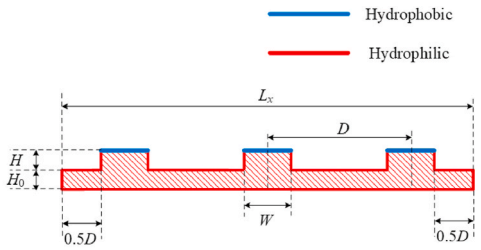

(a) The hydrophilic-hydrophobic mixed surface with micro-pillars

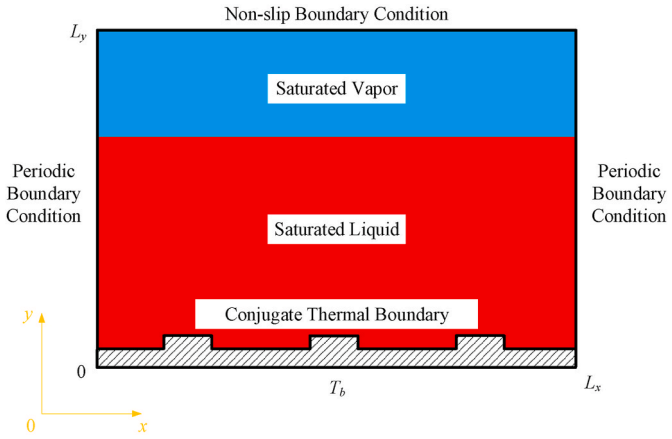

(b) The computational domain

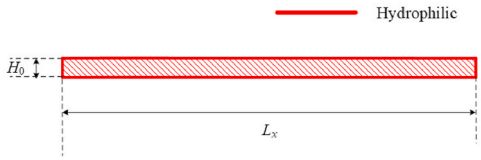

(c) The smooth hydrophilic heated surface

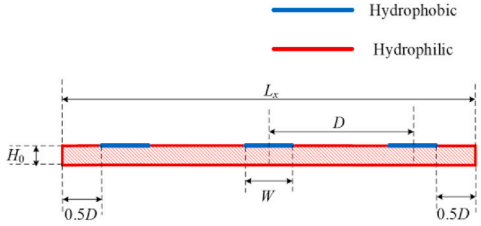

(d) The mixed heated surface without micro-pillars

Fig. 2. The physical model and computational domain.

H_0 and H are fixed as 30 and 6 all the while. Fig. 2(b) represents the computational domain. As shown, the simulations were performed at a rectangular computational domain with a size of $L_x \times L_y = 600 \times 390$. The heated surface in Fig. 2(a) is located at the bottom of the computational domain. To solve the distribution function of density, the periodic boundary condition is adopted at the x-direction, while the non-slip boundary condition is adopted at the top boundary and the solid-fluid interface. The outer wall of the bottom substrate is maintained at a temperature of T_b and the conjugate thermal boundary condition is adopted at the solid-fluid interface to solve the distribution of temperature fields. The parameters in P-R EOS are set as: $a = 3/49$, $b = 2/21$, $R = 1$, $\omega = 0.344$, $T_c = 0.109383$. The relaxation times in Eq. (6) are set as $\tau_\rho = 1$, $\tau_e = 1.25$, $\tau_\varsigma = 1.25$, $\tau_j = 1$ and $\tau_q = 1/1.1$. The parameter σ in Eq. (9) is set as 0.18 and the parameter G in Eq. (11) is set as -1. Initially, the computational domain is occupied by saturated liquid at $H_0 \le y < 250$ and saturated vapor at $250 \le y < L_y$. The saturated temperature is $T_{sat} = 0.9T_c$ and the density of vapor and liquid are $\rho_L = 5.9$ and $\rho_V = 0.58$, respectively. In Eq. (14), κ is set as 0.25, and the surface tension is 0.0885, correspondingly. In Eq. (12), the parameter G_w is set as -0.15 and 0.05 for the hydrophilic and the hydrophobic surfaces, respectively. Correspondingly, the intrinsic contact angles of the hydrophilic and the hydrophobic surfaces are $\theta_b = 57.70°$ and $\theta_t = 100.35°$, respectively. The gravitational acceleration is imposed at the y-direction, $\mathbf{g} = (0, -g_y)$. The physical parameters of the fluid and the heated surface are shown in Table 1. In addition, the pool boiling processes on a smooth hydrophilic heated surface with a contact angle of 57.70° (as shown in Fig. 2(c)) and a hydrophilic-hydrophobic mixed heated surface without micro-pillars (as shown in Fig. 2(d)) are also simulated in this study as comparison groups.

The characteristic length l_0, characteristic velocity v_0 and characteristic time t_0 are defined respectively as Eq. (26). The dimensionless length l^*, dimensionless velocity $\mathbf{v}^*$and dimensionless time t^* are defined as Eq. (27). $Q_{loc}(x, t)$ is the dimensionless local heat flux on the heated surface, $Q_s(t)$ is defined as the dimensionless spatial average heat flux, and Q is defined as the dimensionless temporal and spatial average heat flux, as shown in Eq. (28).

$$l_0 = \sqrt{\frac{\gamma}{g_y(\rho_L - \rho_V)}},\ v_0 = \sqrt{g_y l_0},\ t_0 = \frac{l_0}{v_0} \tag{26}$$

$$l^* = l/l_0,\ \mathbf{v}^* = \mathbf{v}/v_0,\ t^* = t/t_0 \tag{27}$$

$$Q_{loc}(x,t) = -\frac{l_0}{\mu_L h_{fg}}\left(\lambda \nabla_y T\right)\big|_{y=0},\ Q_s(t) = \frac{\int_0^{L_x} Q_{loc}(x,t)dx}{L_x},\ Q = \frac{\int_{t_1}^{t_2} Q_s(t)dt}{t_2 - t_1} \tag{28}$$

4. Results and discussions

4.1. Numerical model validation

During the film boiling processes on a smooth heated surface, the

Table 1
The physical parameters of the fluid and heated surface.

Physical parameters	Saturated liquid	Saturated vapor	Heated surface
Density	$\rho_L = 5.9$	$\rho_V = 0.58$	$\rho_s = 5.9$
Viscosity coefficient	$\nu_L = 0.06$	$\nu_V = 0.06$	/
Specific heat	$c_{v,L} = 8$	$c_{v,V} = 4$	$c_{v,s} = 8$
Thermal diffusion coefficient	$\chi_L = 0.025$	$\chi_V = 0.03$	$\chi_s = 0.5$
Pr	$Pr_L = 2.4$	$Pr_V = 2$	/
Thermal conductivity	$\lambda_L = 1.18$	$\lambda_V = 0.0696$	$\lambda_s = 23.6$
Surface tension	$\gamma = 0.0885$		/
Latent heat	$h_{fg} = 0.4331$		/
Gravitational acceleration	$g_y = 0.00005$		/

temporal and spatial average Nusselt number could be calculated by the expression proposed by Berenson et al. [26], as shown in Eq. (29). According to the definition of Nusselt number, the dimensionless temporal and spatial average heat flux for the film boiling processes could be expressed as Eq. (30). To validate the numerical model used in this study, the film boiling processes on a smooth heated surface were simulated in this section. The physical model shown in Fig. 2(c) and the physical parameters shown in Table 1 are adopted in these simulations, and the numerical results were compared to the analytical solutions given by the expression of Berenson et al. [26].

$$Nu = 0.425 L_x \left[\frac{g_y(\rho_L - \rho_V)h_{fg}}{\lambda_V \mu_V (T_w - T_{sat})}\right]^{1/4} \left[\frac{\gamma}{g_y(\rho_L - \rho_V)}\right]^{-1/8} \tag{29}$$

$$Q = \frac{Nu\lambda_V (T_w - T_{sat})}{L_x^* \mu_L h_{fg}} \tag{30}$$

Fig. 3 represents the evolution of LBM simulated spatial average dimensionless heat flux during film boiling processes at $T_b = 1.11T_c$ and $1.17T_c$, with the comparison with the analytical solutions given by the expression of Berenson et al. [26]. As shown in Fig. 3, the LBM simulated results fluctuate periodically around the analytical solution at each case. When T_b equals $1.11T_c$ and $1.17T_c$, the LBM simulated temporal and spatial dimensionless average heat flux is 0.0366 and 0.0472, respectively, and the corresponding analytical solution given by Eq. (29)~(30) is 0.0414 and 0.0504, respectively. The relative deviations between simulated results and analytical solutions are 11.6% and 6.35%, respectively, in these two cases. The good agreement between the simulated results and the analytical solutions could prove the rationality of the numerical model used in this study.

4.2. The boiling heat transfer on hydrophilic-hydrophobic mixed surface

In this section, the bubble dynamics and heat transfer during pool boiling processes on the hydrophilic-hydrophobic mixed heated surface textured with micro-pillars are simulated and compared to those on the smooth hydrophilic heated surface and the hydrophilic-hydrophobic mixed heated surface without micro-pillars. For the hydrophilic-hydrophobic mixed heated surface with micro-pillars, the pillar width $W^* = 2.741$ and the pillar number $N = 3$.

Fig. 4 represents the evolutions of velocity vectors and vapor bubble patterns during pool boiling processes on these three different types of heated surfaces at $T_b = 0.99T_c$. In this study, the region with $\rho < 0.5(\rho_L + \rho_V)$ was viewed as vapor phase region, i.e., the blue region shown in Fig. 4. As shown in Fig. 4(a), for the hydrophilic-hydrophobic mixed surface with micro-pillars, a vapor bubble is generated on each hydrophobic top at $t^* = 57.95$. On the contrary, there is no bubble nucleated at the bottom substrate with a little higher wall temperature. At $t^* = 66.23$, a "neck" is generated at the bottom of each vapor bubble, indicating that the vapor bubbles tend to depart away from the heated surface with the action of buoyancy force. At $t^* = 71.19$, the vapor bubbles have broken up at the "necks" and departed away from the heated surface. At the same time, a small amount of vapor still remains at the hydrophobic tops and will grow to be new bubbles soon after. As shown Fig. 4(c), the pool boiling processes on the mixed heated surface without micro-pillars at $T_b = 0.99T_c$ are similar to those on the mixed heated surface with micro-pillars. Vapor bubbles continuously nucleate at the hydrophobic regions. At the hydrophilic regions, there is no vapor bubble generates. However, as shown in Fig. 4(b), there is no vapor bubble nucleated on the smooth hydrophilic surface all the time.

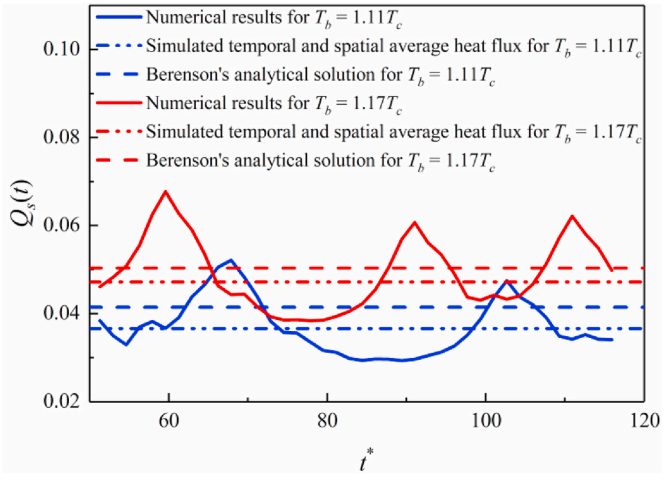

Fig. 3. Comparison of temporal variations of LBM simulated spatial average heat flux in film boiling with Berenson et al.'s analytical solutions [26].

The comparison in Fig. 4 indicates that the hydrophobic regions of the mixed surfaces both with and without micro-pillars benefit to the bubble nucleation and the wall superheat for the onset of nucleate boiling (i.e., ONB) could be reduced obviously. This result could be explained by the heterogeneous nucleation theory of Quan et al. [27] for the smooth heated surface. In addition, through the thermodynamic analysis on location of nucleation sites, Ma et al. [21] have proved that the heterogeneous nucleation theory of Quan et al. [27] could also explain the reason why the bubbles nucleate on the hydrophobic tops of the mixed surface with micro-pillars at a lower wall temperature.

Fig. 5 displays the pool boiling processes on three different types of heated surfaces at $T_b = 1.06T_c$. As shown in Fig. 5(a), vapor bubbles could be generated on both the hydrophobic tops and the bottom substrate of the hydrophilic-hydrophobic mixed surface. Obviously, the number of isolated bubbles on the mixed surface is increased greatly compared to the boiling processes in Fig. 4(a) due to the increasing wall superheat. In addition, the comparison between the boiling processes in Fig. 5(a), (b) and (c) shows that the both pillar structures and wettability have little influence on the number of isolated bubbles on the heated surface when $T_b = 1.06T_c$. On these three different types of heated surfaces, the pool boiling processes fall into the nucleate boiling regime in this case.

Fig. 6 represents the pool boiling processes on three different heated surfaces at $T_b = 1.09T_c$. As shown in Fig. 6(b), the smooth hydrophilic heated surface is covered by a continuous vapor film all the time due to the high wall temperature, and the heat transfer between the heated surface and the bulk liquid is completely obstructed by the vapor film. Obviously, the pool boiling processes on the smooth hydrophilic heated surface in this case fall into the film boiling regime. On the hydrophilic-hydrophobic mixed surface with micro-pillars, as shown in Fig. 6(a), the continuous steam film is unable to be generated. However, some vapor patches are generated at the mixed surface due to the coalescence of the bubbles nucleated at the hydrophobic tops and the bottom substrate. As a result, the whole pillars are covered by the vapor patches, and the heat transfer performance would be decreased compared with that in Fig. 5 (a). As shown in Fig. 6(c), vapor bubbles are generated on both the hydrophilic and the hydrophobic regions continuously, and pool boiling processes fall into the nucleate boiling regime in this case. The comparison between Fig. 6(a), (b) and (c) indicates that both the hydrophilic-hydrophobic mixed surfaces with and without micro-pillars could make the pool boiling processes enter into the film boiling regime at higher wall superheat due to the heterogeneity of wetting property.

Fig. 7(a) represents the pool boiling curves of three different types of heated surfaces. As shown in Fig. 7(a), for the smooth hydrophilic surface, the hydrophilic-hydrophobic mixed surface with micro-pillars and the mixed heated surface without micro-pillars, the outer wall temperatures at ONB are equal to T_c, $0.98T_c$ and $0.98T_c$, respectively, and the boiling processes enter into the film boiling regime at outer wall temperatures with $1.08T_c$, $1.1T_c$ and $1.11T_c$, respectively. Besides, the hydrophilic-hydrophobic mixed surface with micro-pillars possesses the highest heat transfer performance under different wall superheats, as

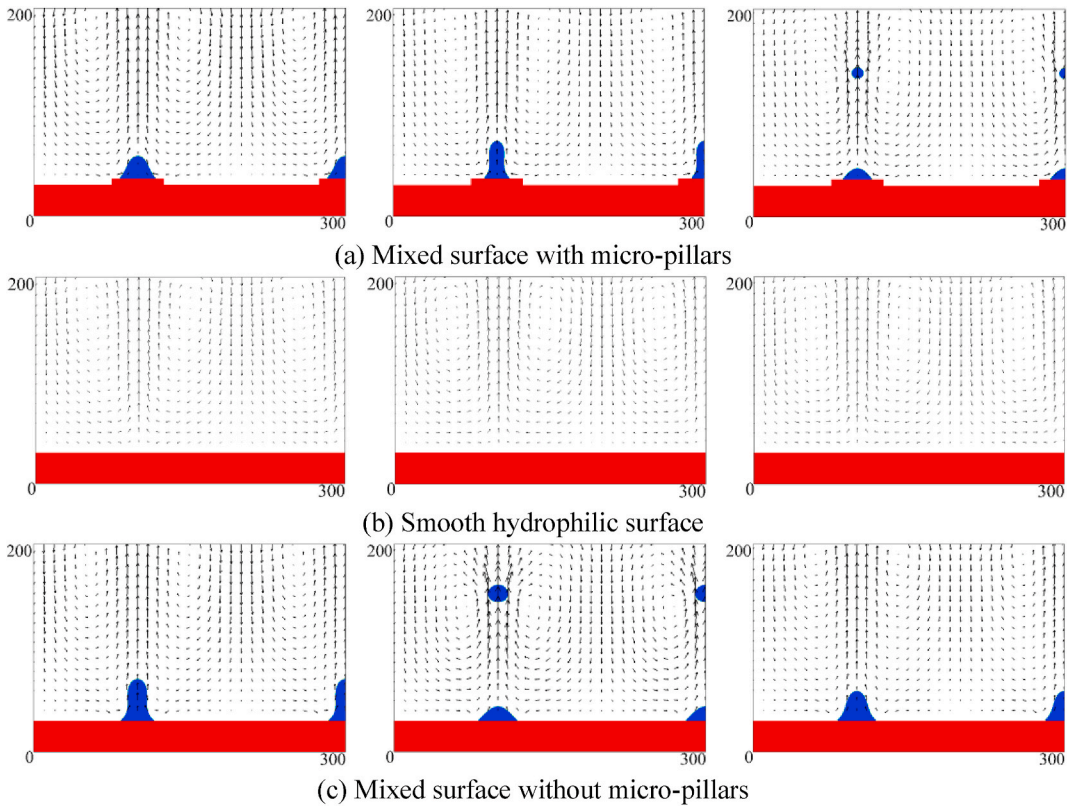

Fig. 4. The evolutions of velocity vectors and bubble patterns during boiling processes on three different types of heated surfaces at $T_b = 0.99T_c$ (From left to right: $t^* = 57.95$, 66.23 and 71.19).

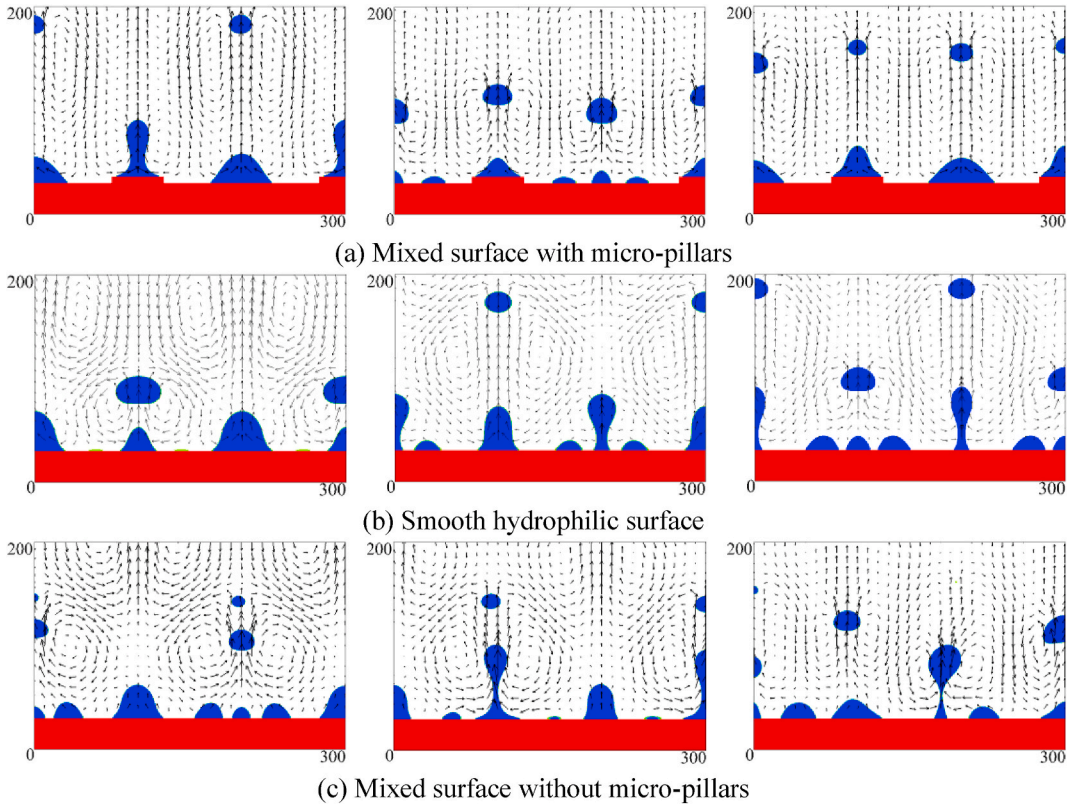

Fig. 5. The evolutions of velocity vectors and bubble patterns during boiling processes on three different types of heated surfaces at $T_b = 1.06T_c$ (From left to right: $t^* = 49.67$, 66.23 and 82.78).

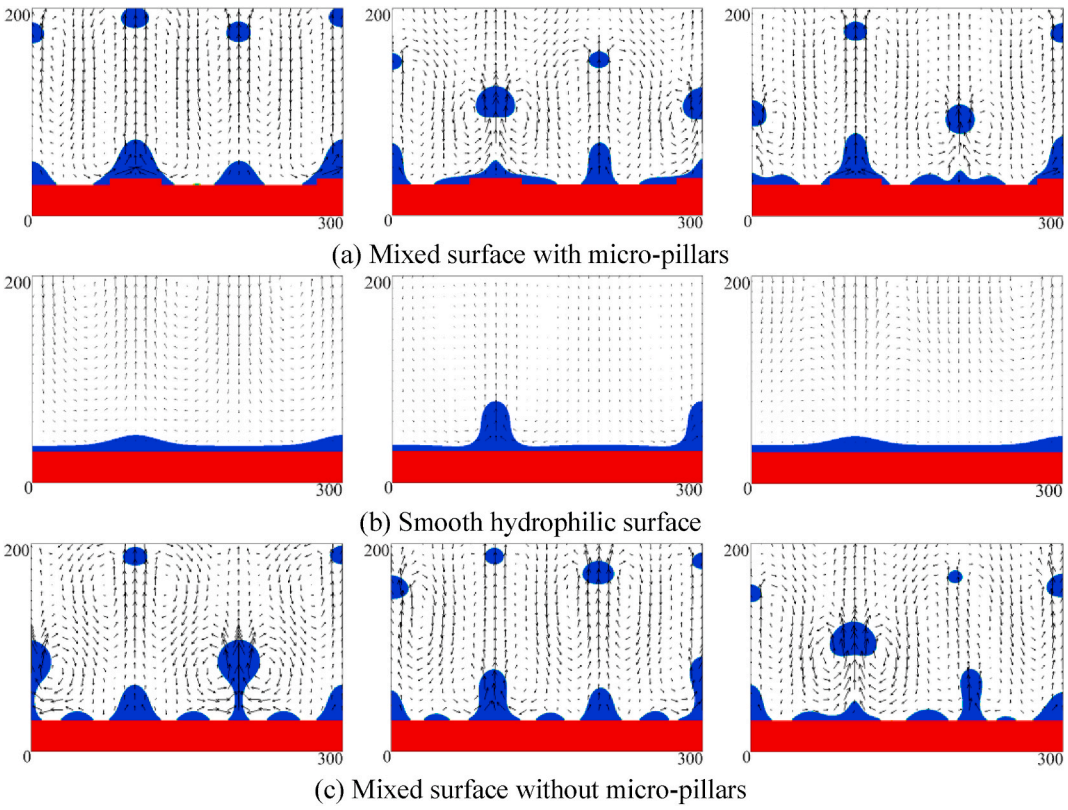

Fig. 6. The evolutions of velocity vectors and bubble patterns during boiling processes on three different types of heated surfaces at $T_b = 1.09T_c$ (From left to right: $t^* = 49.67$, 66.23 and 82.78).

well as the CHF, compared to the other two types of heated surfaces. However, the hydrophilic-hydrophobic mixed surface with micro-pillars would slightly reduce the wall superheat at the CHF point compared with the smooth hydrophilic surface. On the other hand, the hydrophilic-hydrophobic mixed surface without micro-pillars could also enhance the heat transfer performance compared to the smooth hydrophilic surface when wall superheat is low (i.e., $T_b \leq 1.03T_c$). However, in the nucleate boiling regime with high wall superheat and in the film boiling regime, the boiling curves of these two types of heated surfaces are almost coincident. The numerical results in Fig. 7(a) indicate that both the existence of pillar structures and the heterogeneity of wetting property are important factors for improving the boiling heat transfer performance when wall superheat is low. However, the existence of pillar structures, rather than the heterogeneity of wetting property, becomes the main impact for improving the heat transfer performance in the nucleate boiling regime with high wall superheat and in the film boiling regime.

Fig. 7(b) represents the percentage enhancement in the boiling heat transfer performance of the hydrophilic-hydrophobic mixed surfaces with and without micro-pillars compared with the smooth hydrophilic surface in the nucleate boiling regime (i.e., $0.99 \leq T_b/T_c \leq 1.07$) and the film boiling regime (i.e., $T_b/T_c \geq 1.11$). $r_{en} = (Q_{mix} - Q_{smo})/Q_{smo}$, Q_{mix} and Q_{smo} are the temporal and spatial average dimensionless heat flux for the hydrophilic-hydrophobic mixed surfaces and the smooth hydrophilic surface, respectively. As shown in Fig. 7(b), for both the hydrophilic-hydrophobic mixed surfaces with and without micro-pillars, the percentage enhancement decreases with an increase in outer wall temperature in the nucleate boiling regime, and this result is consistent with the experimental results of Kumar et al. [9]. In addition, in the film boiling regime, it's found that the mixed surface with micro-pillars produces a percentage enhancement of about 30% in boiling heat transfer performance compared to the smooth hydrophilic surface at a given outer wall temperature.

4.3. The influence of pillar width

In this section, simulations of pool boiling processes on the hydrophilic-hydrophobic mixed surfaces with different pillar widths are performed to investigate the influence of pillar width on bubble dynamics and heat transfer during pool boiling processes. In these simulations, the pillar number of these heated surfaces is fixed as $N = 3$, while the pillar pitch distances are $W^* = 0.548$, $W^* = 1.644$, $W^* = 2.741$, $W^* = 5.482$ and $W^* = 8.224$, respectively. Obviously, the increasing pillar width means an increase in the area of hydrophobic regions on the tops of the pillars and a decrease in the hydrophilic area on the bottom of the heated surface.

Fig. 8(a) represents the evolution of bubble contours during pool boiling processes on the hydrophilic-hydrophobic mixed surfaces with $W^* = 1.644$ and 5.482 at a low outer wall temperature ($T_b = 0.99T_c$). In this study, the bubble contours represent the regions with $\rho = 0.5(\rho_L + \rho_V)$. As shown in Fig. 8(a), in both cases, the vapor bubbles are nucleated at the hydrophobic tops, and the boiling processes fall into the partial nucleate boiling regime. For the hydrophilic-hydrophobic mixed surface with $W^* = 1.644$, a vapor bubble is generated on each hydrophobic top at $t^* = 13.25$. With the growth of these vapor bubbles, the bubble size increases greatly and these vapor bubbles finally depart away from the heated surface at $t^* = 33.11$. For the hydrophilic-hydrophobic mixed surface with $W^* = 5.482$, the first-generation bubbles are also nucleated on the heated surface at $t^* = 13.25$. However, it can be seen from Fig. 8 (a) that there are two vapor bubbles nucleated on each hydrophobic top when $W^* = 5.482$. With the growth of these two vapor bubbles, they finally merge with each other to generate a large vapor bubble. Since the large bubble size leads to large buoyancy force, the first-generation bubbles depart away from the heated surface at $t^* = 29.80$. In other words, compared with the mixed surfaces with $W^* = 5.482$, the first-generation bubbles spend more time in growing on the mixed surfaces with $W^* = 1.644$.

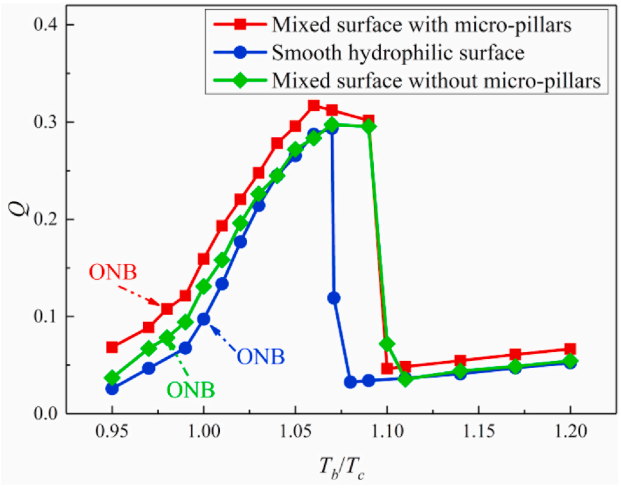

(a) Boiling curves

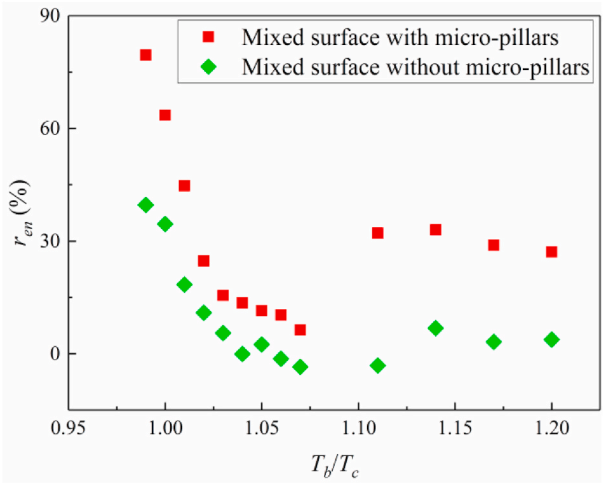

(b) Percentage enhancement in boiling heat transfer performance

Fig. 7. Comparison of boiling heat transfer performance under different outer wall temperatures between the three different types of heated surfaces.

Fig. 8(b) represents the evolution of the dimensionless equivalent diameter of the vapor bubbles which are growing on each hydrophobic top of the mixed surface during pool boiling with $T_b = 0.99T_c$. As shown in Fig. 8(b), for each case, the bubble equivalent diameter equals 0 until small vapor bubbles are nucleated on the hydrophobic tops. After that, the bubble equivalent diameter increases gradually. When the vapor bubble departs away from the mixed surface, the bubble equivalent diameter decreases suddenly but is still greater than 0 because a small amount of vapor remains on the hydrophobic tops. Then the residual vapor will grow to be a new vapor bubble, and the bubble equivalent diameter increases until the new vapor bubble departs away. It could be concluded from Fig. 8 that the bubble release frequency and average bubble size during the pool boiling processes increase with an increase in pillar width because the hydrophobic tops benefit the bubble nucleation processes. It means that the vapor bubbles could carry more thermal energy away from the heated surface, and it could be inferred that the heat transfer performance is enhanced by the increasing pillar width when the wall superheat is low. This conjecture could be confirmed by Fig. 9, which represents the evolution of spatial average dimensionless heat flux during the pool boiling on the mixed heated surface with different pillar widths in this case. In addition, it can be seen from Fig. 9 that pool boiling performance of the mixed surface with $W^* = 1.644$ is much lower than that of others in this case. This result is caused by that there is no vapor bubbles nucleated on the hydrophobic tops of the mixed surface with $W^* = 1.644$ all the while, but the boiling processes on all of the other mixed surfaces fall into the nucleate boiling regime.

Moreover, Fig. 10 gives the distribution of bubble contours during pool boiling processes on the hydrophilic-hydrophobic mixed surfaces with different pillar widths in the cases of various wall superheats. It's found from Fig. 10 that the outer wall temperature at ONB increases with a decrease in pillar width when $W^* \leq 1.644$. Especially, for the mixed surface with a pillar width of $W^* = 0.548$, the outer wall temperature at ONB has become same as that of the smooth hydrophilic heated surface with the contact angle of 57.70°, and the vapor bubbles are generated preferentially on the bottom substrate rather than the hydrophobic tops. It indicates that the hydrophobic tops would not promote the bubble nucleation processes at a low wall superheat if the pillar width is too small.

Fig. 11(a) represents the distribution of bubble contours during pool boiling processes on the hydrophilic-hydrophobic mixed surfaces with different pillar widths when $T_b = 1.06T_c$. As shown in Fig. 11(a), vapor bubbles could be generated on both the hydrophobic tops and the bottom substrate. When $W^* = 2.741$, the average number of isolated bubbles on the bottom substrate is greater than that on the hydrophobic tops, obviously. However, when $W^* = 5.482$ and 8.224, the average number of isolated bubbles on the bottom substrates of the mixed surfaces is much less than that of mixed surface with $W^* = 2.741$. This result indicates that the larger pillar width would impede the nucleation of vapor bubbles on the bottom substrate to some extent. Fig. 11(b) represents the evolution of spatial average wetted area fraction and number of isolated bubbles on the mixed heated surface during pool boiling processes with $T_b = 1.06T_c$. It can be seen from Fig. 11(b) that both the average wetted area fraction and number of isolated bubbles on the mixed heated surface stays almost unchanged when $W^* \leq 2.741$ and decreases obviously with an increase in pillar width when $W^* > 2.741$. This result is caused by two reasons. On the one hand, it's easier for the hydrophobic tops to be covered by the vapor phase, thus the average wetted area fraction is reduced with an increase in pillar width. On the other hand, when $W^* > 2.741$, the larger pillar width would hinder the nucleation of vapor bubbles on the bottom substrate to some extent, as shown in Fig. 11(a), and thus the average number of isolated bubbles is decreased a lot. Especially, as shown in Fig. 11(a), when $W^* = 8.224$, the vapor bubbles nucleated on the bottom substrate merge with those nucleated on the hydrophobic top, and this result causes the average wetted area fraction and the number of isolated bubbles on the mixed heated surface to be very small.

Fig. 12 represents the influence of pillar width on heat transfer performance during boiling processes on the hydrophilic-hydrophobic mixed surfaces when $T_b = 1.06T_c$. It could be concluded from Figs. 11 and 12 that the wetted area fraction and number of isolated bubbles on the mixed heated surfaces have a dominant influence on heat transfer performance during the pool boiling processes at the given outer wall temperature of $T_b = 1.06T_c$. Therefore, the mixed surfaces with $W^* = 5.482$ and 8.224 have worse heat transfer performance compared with other mixed surfaces. In addition, it can be seen from Fig. 12(b) that the heat transfer performance of the mixed surfaces increases firstly and then decreases gradually with an increase in pillar width, and the mixed surface with $W^* = 1.644$ possesses the highest heat transfer performance in the case of $T_b = 1.06T_c$.

In Ref. [12], Li et al. found that heat transfer performance in the nucleate boiling regime with high wall superheat decreases as the increase in pillar width. However, it seems that an opposite conclusion was obtained by Ma et al. [21]. In fact, both of their conclusions are rational but one-sided. The mixed surfaces with $W^* \geq 0.915$ were adopted in Ref. [12]. While in Ref. [21], only two mixed surfaces with $W^* = 1.41$ and 0.45 were utilized. The numerical results in this study are qualitatively consistent with those in both Ref. [12] and Ref. [21] and could explain the "contradiction" between the numerical results in these

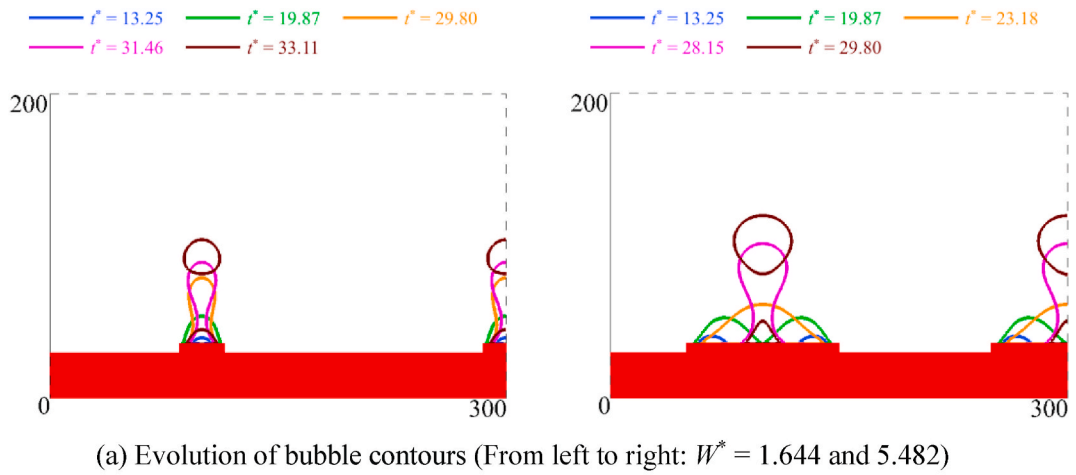

(a) Evolution of bubble contours (From left to right: W^* = 1.644 and 5.482)

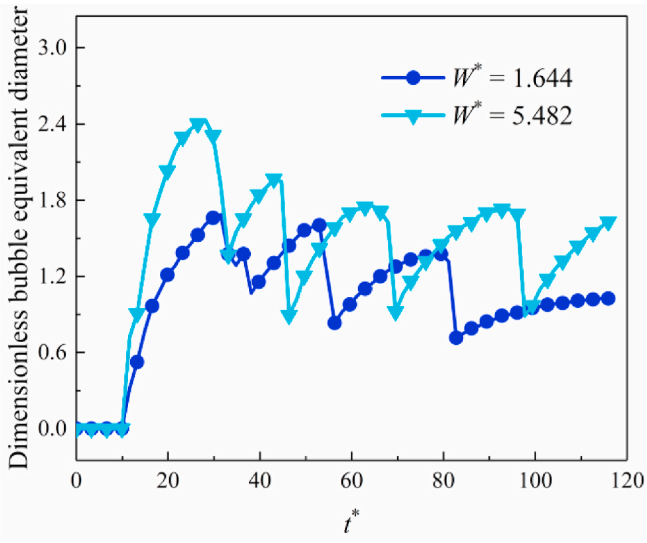

(b) Evolution of dimensionless equivalent diameter

Fig. 8. The bubble dynamics during pool boiling processes on the hydrophilic-hydrophobic mixed surfaces with different pillar widths at $T_b = 0.99T_c$.

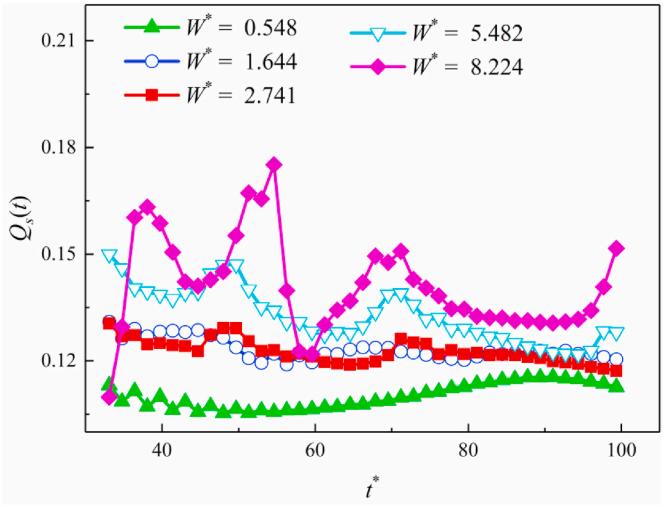

Fig. 9. The evolution of spatial average dimensionless heat flux during the pool boiling on the mixed heated surface with different pillar widths when $T_b = 0.99T_c$.

two literature.

Fig. 13 represents the influence of pillar width on boiling curves of hydrophilic-hydrophobic mixed surfaces. As shown in Fig. 13, for the nucleate boiling processes with a low outer wall temperature ($0.98T_c \leq T_b \leq 0.99T_c$), heat transfer performance of the mixed surface increases with an increase in pillar width. It's because the increasing pillar width benefits the nucleation, growth and departure of the vapor bubbles on the hydrophobic tops, as shown in Fig. 8–10. Since the wall superheat is low, the vapor bubbles could hardly nucleate on the bottom substrate, and the heat transfer performance is dominated by the bubble dynamics on hydrophobic tops. Therefore, the hydrophilic-hydrophobic mixed surface with larger pillar width possesses higher boiling heat transfer performance when wall temperature is low. However, in the nucleate boiling regime with a high outer wall temperature (i.e., $T_c \leq T_b \leq 1.06T_c$), boiling heat transfer performance increases firstly and then decreases with an increase in pillar width, and the mixed surface with $W^* = 1.644$ possesses the maximum heat transfer performance, as well as the largest CHF. The reason has been explained in Figs. 11 and 12. In addition, it can be seen from Fig. 13 that the pillar width has little influence on boiling heat transfer performance in the film boiling regime because the total heat exchange area stays unchanged.

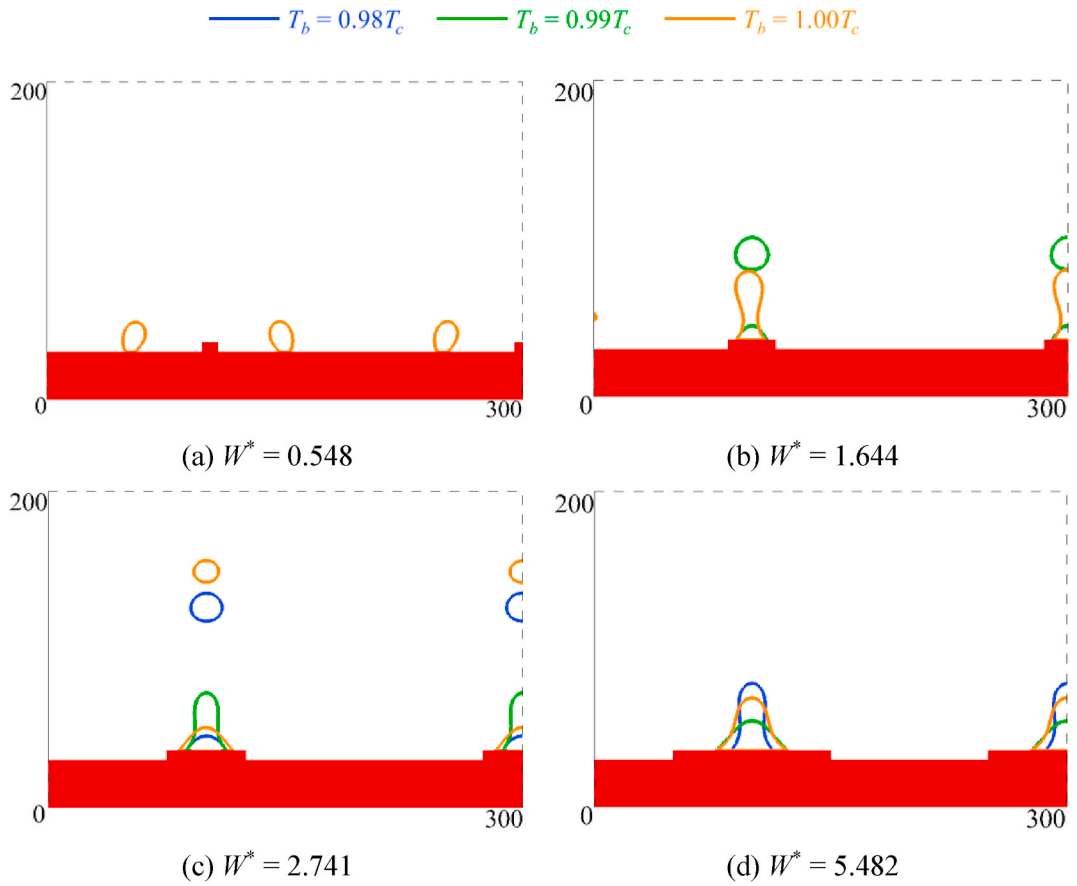

Fig. 10. The distribution of bubble contours during pool boiling processes on the hydrophilic-hydrophobic mixed surfaces with different pillar widths in the cases of various wall superheats.

4.4. The influence of pillar number

To investigate the influence of pillar number on pool boiling heat transfer, simulations of boiling heat transfer on hydrophilic-hydrophobic mixed surfaces with different pillar number are performed in this section. The pillar width of these heated surfaces is fixed as $W^* = 2.741$, and the pillar number is set as $N = 2$, $N = 3$, $N = 4$, $N = 6$, $N = 8$ and $N = 10$, respectively. Obviously, the increase in pillar number means a decrease in pillar pitch distance and a decrease in the hydrophilic area on the bottom substrate.

Fig. 14(a) represents the boiling curves of hydrophilic-hydrophobic mixed surfaces with different pillar number. As shown in Fig. 14(a), the pillar number has an obvious effect on the boiling heat transfer performance of hydrophilic-hydrophobic mixed surfaces under different wall superheats. Generally speaking, the increasing pillar number could make the boiling curve move to the upper left. In the nucleate boiling regime with lower wall superheat (i.e., $0.98T_c \leq T_b \leq 1.01T_c$), heat transfer performance increases with an increase in pillar number. However, the outer wall temperature at the CHF point decreases with an increase in pillar number. For example, for the hydrophilic-hydrophobic mixed surfaces with $N = 2$, 4 and 8, CHF occurs at the outer wall temperatures of $T_b = 1.07T_c$, $1.06T_c$ and $1.03T_c$, respectively. In addition, the mixed surfaces with $N = 2$ and 10 possess the relative lower CHF compared with other mixed surfaces, and pillar number has little influence on CHF when $3 \leq N \leq 8$. Besides, it can be seen from Fig. 14 that the pillar number has little influence on boiling heat transfer performance in the film boiling regime. When $N \leq 6$, for the mixed surfaces with different pillar numbers, the boiling processes enter into the film boiling regime at almost a constant outer wall temperature with $T_b = 1.1T_c$. However, when $N \geq 8$, the boiling processes enter into the film boiling regime at a lower wall superheat for the mixed surface with a larger pillar number. Considering the heat transfer coefficients under different wall superheats and CHF, it's rational to believe that the mixed surface with $N = 8$ possesses the highest heat transfer performance.

Fig. 14(b) represents the quantitative influence of pillar number on nucleate boiling heat transfer, in which $Q(N = 3)$ is the average heat flux of the mixed surface with pillar number of $N = 3$ under different wall superheats. As shown in Fig. 14(b), the pillar number has different influence on boiling heat transfer coefficient under different outer wall temperatures. For example, when $T_b = 0.99T_c$, average heat flux of mixed surfaces with pillar number of $N = 2$, 4, 6, 8 and 10 equals to 0.81, 1.22, 1.60, 1.74 and 1.77 times as much as that of mixed surface with $N = 3$. In this case, increasing the pillar number would enhance the heat transfer efficiency. When outer wall temperature is increased to be $1.05T_c$, average heat flux of mixed surfaces with pillar number of $N = 2$, 4, 6, 8 and 10 equals to 0.94, 1.03, 1.10, 0.98 and 0.53 times as much as that of mixed surface with $N = 3$. The numerical results in the case of $T_b = 1.05T_c$ indicate that increasing pillar number would reduce the heat transfer when outer wall temperature is high and the pillar number exceeds a certain value.

Fig. 15 represents the bubble dynamics during pool boiling processes on the hydrophilic-hydrophobic mixed surfaces with different pillar number at $T_b = 0.99T_c$. As shown in Fig. 15, for all of these cases, a vapor bubble is generated on each hydrophobic top and there is no vapor bubble nucleated at the bottom substrate. With an increase in pillar number, the number of isolated bubbles on the mixed surface increases because the hydrophobic tops benefit to bubble nucleation. Due to the low wall superheat, the growth and departure of vapor bubbles are independent with those of each other, and the increasing number of isolated bubbles on the mixed surface would enhance the pool boiling heat

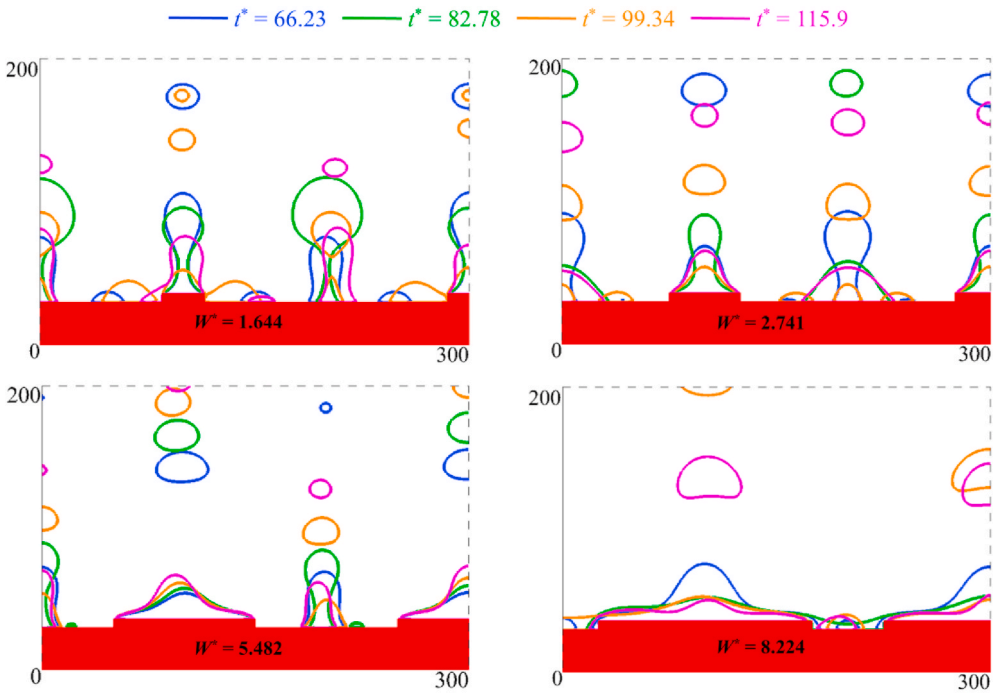

(a) Bubble contours

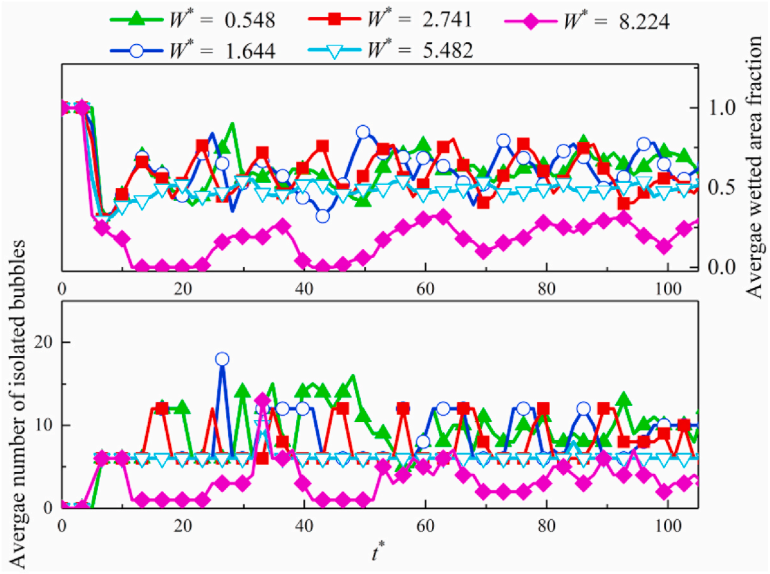

(b) Spatial average wetted area fraction and number of isolated bubbles

Fig. 11. The evolution of bubble contours, spatial average wetted area fraction and number of isolated bubbles on the hydrophilic-hydrophobic mixed surfaces with different pillar widths during pool boiling processes when $T_b = 1.06T_c$.

transfer performance. Therefore, the pool boiling heat transfer performance increases with an increase in pillar number when the wall superheat is low, as shown in Fig. 14.

Fig. 16(a) represents the evolution of bubble contours during pool boiling processes on the hydrophilic-hydrophobic mixed surfaces with different pillar number at $T_b = 1.02T_c$. As shown in Fig. 16(a), when $N \leq 4$, the vapor bubbles could be generated on both the hydrophobic tops and the bottom substrate. However, when $N = 6$, it can be seen that the vapor bubbles are generated only on the hydrophobic tops, indicating that the bubble nucleation processes on the bottom substrate would be prevented by the decreasing pillar pitch distance as the pillar number increases. In addition, it can be seen from Fig. 16(a) that the interaction between the vapor bubbles is weak for the mixed surfaces with $N \leq 6$. However, when $N = 8$, the vapor bubbles nucleated on the hydrophobic tops have a tendency of merging with others. Further, when N is increased to 10, sometimes vapor patches are generated on the heated surface due to the coalescence of vapor bubbles, and some of the cavities between the adjacent pillars would be filled with vapor. Fig. 16(b) gives the influence of pillar number on temporal and spatial average wetted area fraction, number of isolated bubbles and dimensionless heat flux. As shown in Fig. 16(b), with an increase in pillar number, average wetted area fraction decreases, while the numbers of isolated bubbles increases gradually because the hydrophobic tops benefit to bubble nucleation. On the other hand, as the pillar number increases, boiling

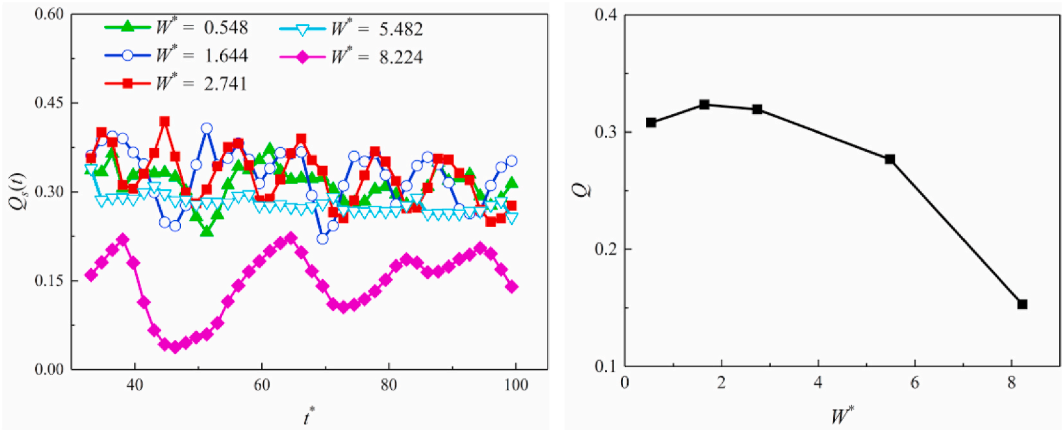

(a) $Q_s(t)$ versus t^* under various pillar widths (b) Q versus W^*

Fig. 12. The influence of pillar width on heat transfer performance during boiling processes on the hydrophilic-hydrophobic mixed surfaces when $T_b = 1.06T_c$.

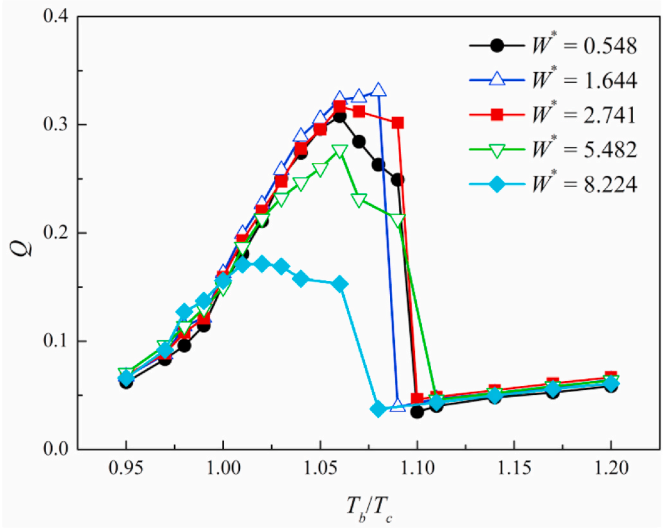

Fig. 13. The influence of pillar width on boiling curves of hydrophilic-hydrophobic mixed surfaces.

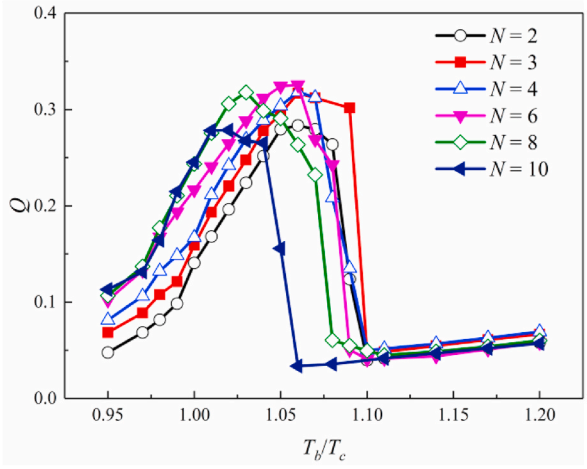

(a) The influence of pillar number on boiling curves

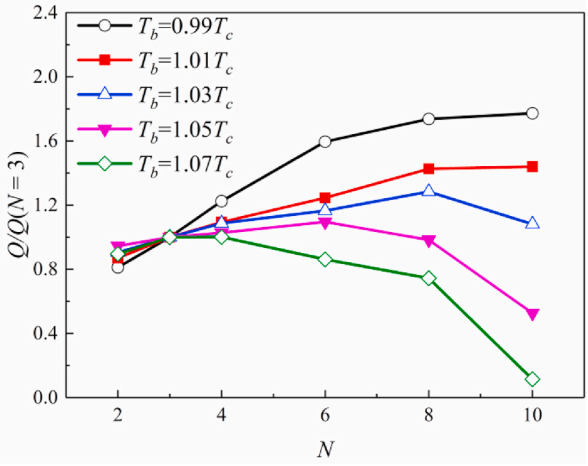

(b) The influence of pillar number on nucleate boiling heat transfer

Fig. 14. The influence of pillar number on pool boiling heat transfer performance of hydrophilic-hydrophobic mixed surfaces.

heat transfer performance in this case is enhanced gradually when $N \leq 8$ but reduced suddenly when $N = 10$. Obviously, the sudden decrease in boiling heat transfer performance when $N = 10$ is caused by that vapor patches are generated on the mixed surface, as shown in Fig. 16(a).

Fig. 17(a) represents the bubble dynamics during pool boiling processes on the hydrophilic-hydrophobic mixed surfaces with different pillar number at $T_b = 1.06T_c$. Correspondingly, Fig. 17(b) gives the influence of pillar number on temporal and spatial average wetted area fraction, the number of isolated bubbles and dimensionless heat flux. As shown in Fig. 17(a), when $N \leq 6$, vapor bubbles are nucleated on both the hydrophobic tops and the bottom substrate, and these vapor bubbles always merge with others to form large bubbles before departing away from the heated surface. As shown in Fig. 17(b), when $N \leq 6$, pillar number has little influence on number of isolated bubbles and wetted area fraction on the mixed surface, as well as the boiling heat transfer performance. However, when $N \geq 8$, it can be seen from Fig. 17(a) that some of the cavities between the adjacent pillars are completely filled with vapor phase. Especially, when $N = 10$, a continuous vapor film is generated on the whole heated surface all the time, and the boiling processes fall into the film regime at this case. Therefore, average wetted area fraction and number of isolated bubbles on the mixed surface, as well as the boiling heat transfer performance are decreased gradually when $N \geq 8$, as shown in Fig. 17(b). Both Figs. 16(c) and Fig. 17(c) indicate that when $T_b \geq 1.02T_c$, boiling heat transfer performance of the mixed surface would decrease suddenly with an increase in the pillar

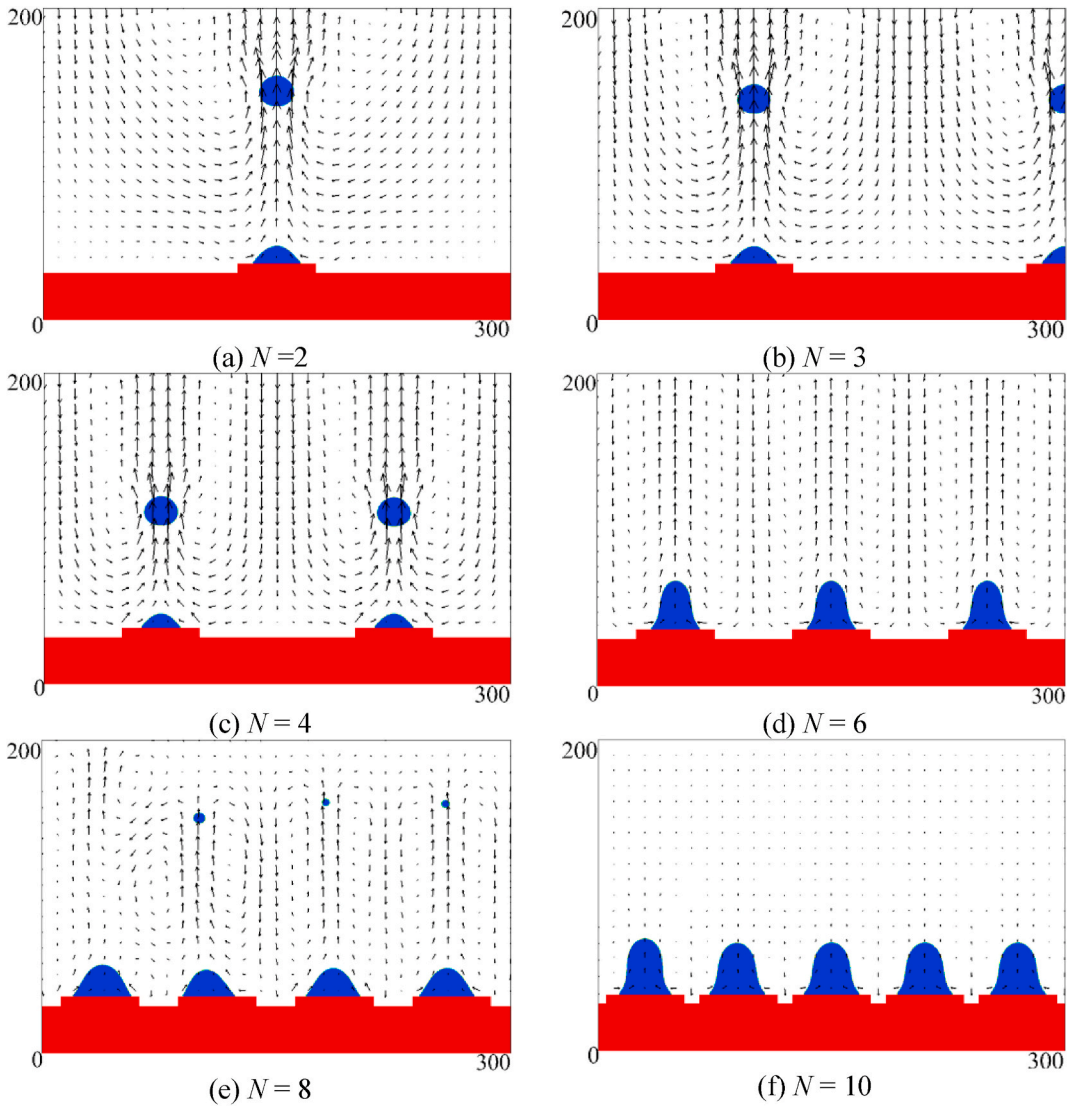

Fig. 15. The bubble dynamics during pool boiling on the hydrophilic-hydrophobic mixed surfaces with different pillar number at $T_b = 0.99T_c$.

number if the pillar number exceeds a certain value. Besides, with an increase in wall superheat, the certain value decreases gradually.

5. Concluding remarks

Using the MRT pseudopotential LB model coupled with liquid-vapor phase-change model, the pool boiling processes on the hydrophilic-hydrophobic mixed surface textured with micro-pillars were simulated and compared with those on the smooth hydrophilic surface and the hydrophilic-hydrophobic mixed surface without micro-pillars. Based on these results, the mechanism of heat transfer enhancement of the mixed surface with micro-pillars was revealed. Besides, the influence of the geometrical parameters of micro-pillars, including pillar widths and pillar number, on bubble dynamics and heat transfer during pool boiling processes of the mixed surface were analyzed in detail. The main findings and conclusions are summarized as follows.

1) In the nucleate boiling regime with low outer wall temperature, the hydrophilic-hydrophobic mixed surface with micro-pillars possesses the highest boiling heat transfer coefficient, and the smooth hydrophilic surface possesses the lowest one. This result indicates that the both existence of pillar structures and heterogeneity of wetting property could enhance the heat transfer performance of the mixed surfaces in this case. Besides, the percentage enhancement in boiling heat transfer performances of the mixed surfaces both with and without micro-pillars compared to the smooth hydrophilic surface decrease gradually with an increase in outer wall temperature.
2) In the nucleate boiling regime with high wall superheat and the film boiling regime, the hydrophilic-hydrophobic mixed surface with micro-pillars still possesses the highest heat transfer coefficient, while the heat transfer coefficient of the mixed surface without micro-pillars is almost equal to that of the smooth hydrophilic surface. This result indicates that existence of pillar structures, rather than the heterogeneity of wetting property, could enhance the heat transfer performance of the mixed surfaces in this case. Even though, the heterogeneity of wetting property could hinder the formation of continuous vapor film on the heated surface to some extent.
3) Since the hydrophobic tops benefit the nucleation of vapor bubbles, bubble release frequency, average bubble size and heat transfer performance decreases with a decrease in pillar width during the nucleate boiling processes with low wall superheat. In addition, it is found that the hydrophobic tops wouldn't promote the bubble nucleation if the pillar width is too small ($W^* = 0.548$). However, in the nucleate boiling regime with high wall superheat, boiling heat transfer performance increases firstly and then decreases with an increase in pillar width, and the mixed surface with $W^* = 1.644$

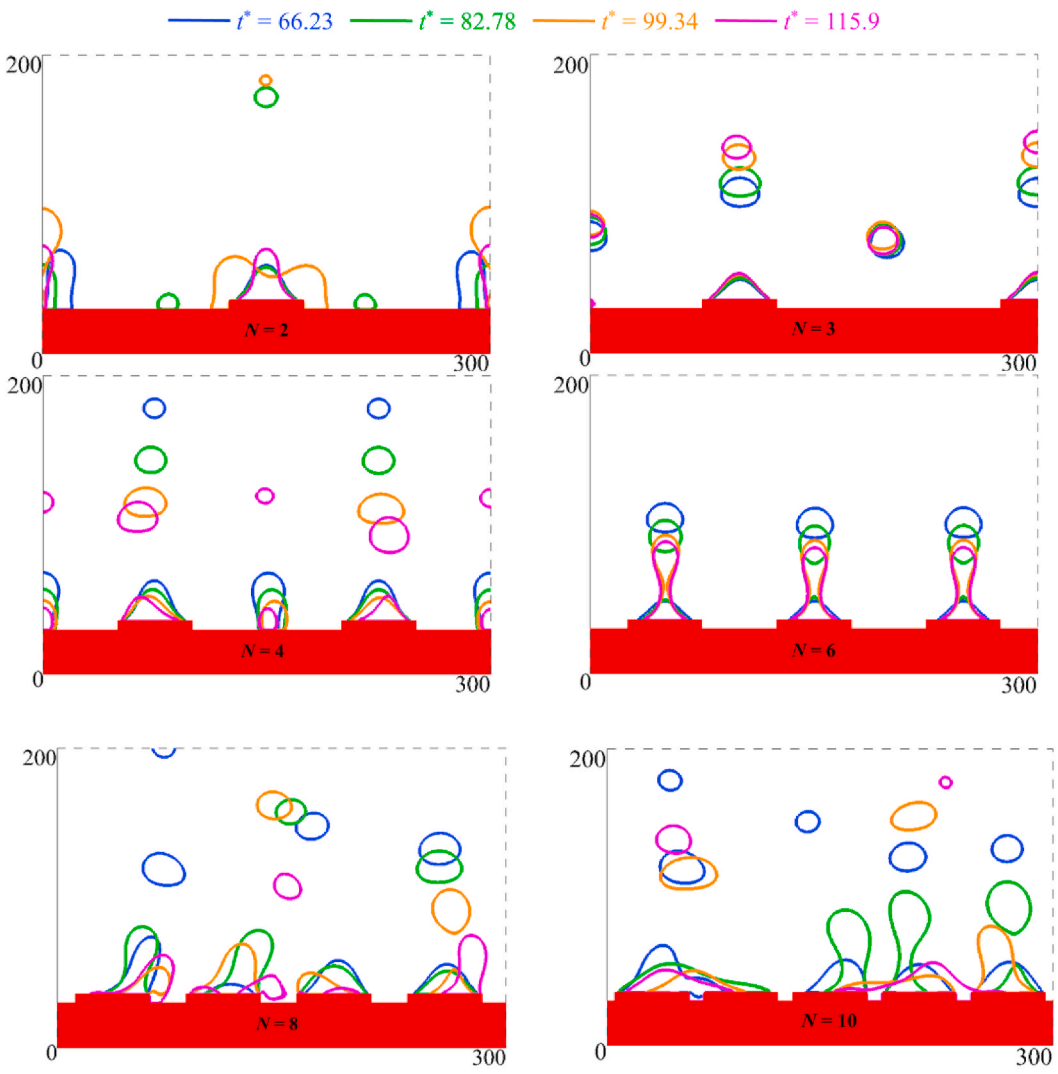

(a) The evolution of bubble contours

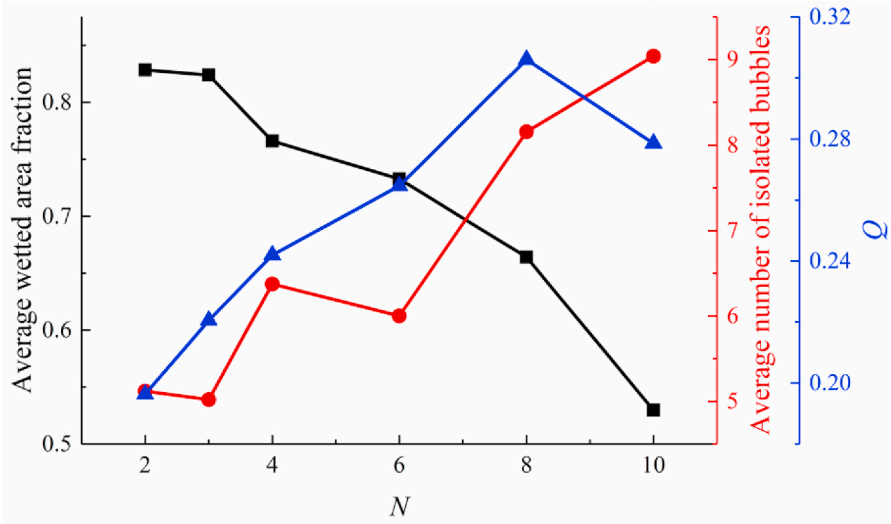

(b) The influence of N on temporal and spatial average wetted area fraction, number of isolated bubbles and dimensionless heat flux

Fig. 16. The bubble dynamics and heat transfer during pool boiling on the hydrophilic-hydrophobic mixed surfaces with different pillar number when $T_b = 1.02T_c$.

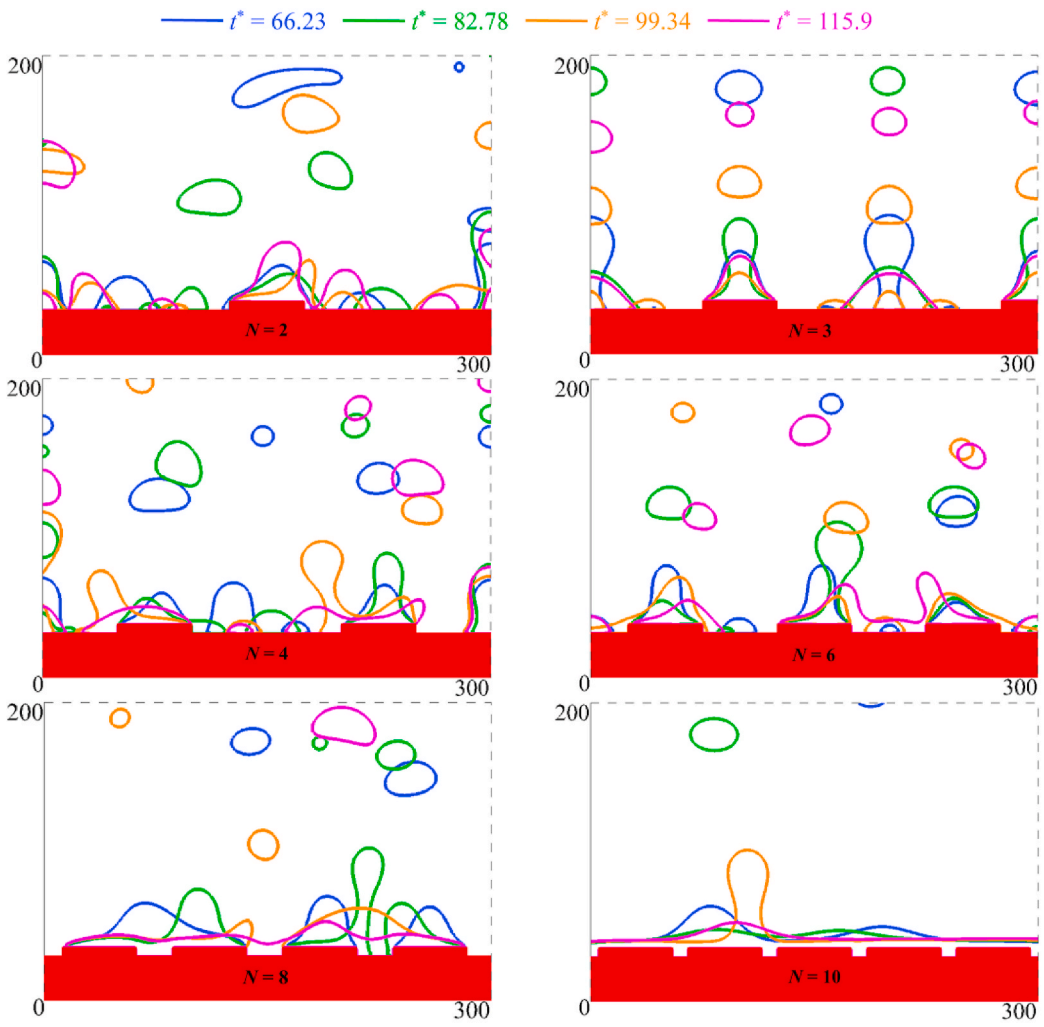

(a) The evolution of bubble contours

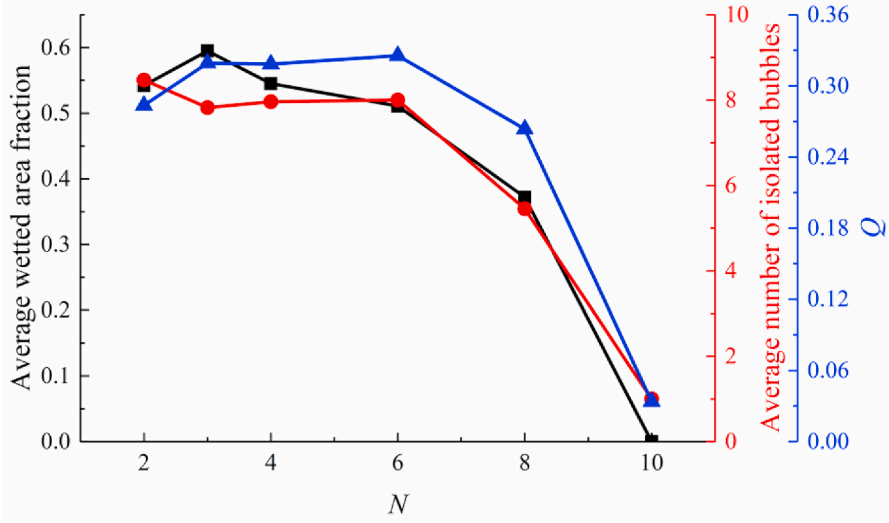

(b) The influence of N on temporal and spatial average wetted area fraction, number of isolated bubbles and dimensionless heat flux

Fig. 17. The bubble dynamics and heat transfer during pool boiling on the hydrophilic-hydrophobic mixed heated surfaces with different pillar number at $T_b = 1.06T_c$.

possesses the maximum heat transfer performance, as well as the largest CHF. Besides, the pillar width has little effect on heat transfer performance in the film boiling regime.

4) As the pillar number increases, the boiling curve would be shifted to the upper left. In the nucleate boiling regime with low wall superheat, pool boiling heat transfer performance is enhanced by increasing pillar number due to the increasing number of isolated bubbles on the heated surface. In the nucleate boiling regime with higher wall superheat ($T_b \geq 1.02T_c$), with an increase in pillar number, boiling heat transfer performance increases firstly and then decreases drastically. It's because that vapor patches or even vapor film would be generated on the mixed heated surface if the pillar number exceeds a certain value, and thus the heat transfer performance of mixed surface would be reduced. Besides, it's found that this certain value decreases gradually with an increase in wall temperature when $T_b \geq 1.02T_c$. Considering the heat transfer coefficients under different wall superheats and CHF, it's found that the mixed surface with $N = 8$ possesses the best heat transfer performance.

Declaration of competing interest

The authors declare that they have no known competing financial interests or personal relationships that could have appeared to influence the work reported in this paper.

Acknowledgement

This work was supported financially by the joint fund between the Chinese Academy of Sciences (CAS) and National Natural Science Foundation of China (NSFC) under the Grant of U1738105.

References

[1] S. Siedel, Bubble Dynamics and Boiling Heat Transfer : a Study in the Absence and in the Presence of Electric Fields, INSA de Lyon, 2012.
[2] D. Lee, J.-S. Lim, N. Lee, H.H. Cho, Enhanced thermal uniformity and stability in pool boiling heat transfer using ultrasonic actuation, Int. Commun. Heat Mass Tran. 106 (2019) 22–30.
[3] K. Guo, H. Li, Y. Feng, T. Wang, J. Zhao, Numerical simulation of magnetic nanofluid (MNF) film boiling using the VOSET method in presence of a uniform magnetic field, Int. J. Heat Mass Tran. 134 (2019) 17–29.
[4] K. Guo, H. Li, Y. Feng, T. Wang, J. Zhao, Enhancement of non-uniform magnetic field on saturated film boiling of magnetic nanofluid (MNF), Int. J. Heat Mass Tran. 143 (2019) 118594.
[5] J.J. Wei, H. Honda, Effects of fin geometry on boiling heat transfer from silicon chips with micro-pin-fins immersed in FC-72, Int. J. Heat Mass Tran. 46 (21) (2003) 4059–4070.
[6] A. Betz, J. Xu, H. Qiu, D. Attinger, Do surfaces with mixed hydrophilic and hydrophobic areas enhance pool boiling? Appl. Phys. Lett. 97 (14) (2010) 103115.
[7] H. Jo, H.S. Ahn, S. Kang, M.H. Kim, A study of nucleate boiling heat transfer on hydrophilic, hydrophobic and heterogeneous wetting surfaces, Int. J. Heat Mass Tran. 54 (25) (2011) 5643–5652.
[8] B.J. Suroto, M. Tashiro, S. Hirabayashi, S. Hidaka, M. Kohno, Y. Takata, Effects of hydrophobic-spot periphery and subcooling on nucleate pool boiling from a mixed-wettability surface, J. Therm. Sci. Technol. 8 (1) (2013) 294–308.
[9] C.S. Sujith Kumar, Y.W. Chang, P.-H. Chen, Effect of heterogeneous wettable structures on pool boiling performance of cylindrical copper surfaces, Appl. Therm. Eng. 127 (2017) 1184–1193.
[10] C. Zhang, L. Zhang, H. Xu, P. Li, B. Qian, Performance of pool boiling with 3D grid structure manufactured by selective laser melting technique, Int. J. Heat Mass Tran. 128 (2019) 570–580.
[11] R.J. MacNamara, T.L. Lupton, R. Lupoi, A.J. Robinson, Enhanced nucleate pool boiling on copper-diamond textured surfaces, Appl. Therm. Eng. 162 (2019) 114145.
[12] Q. Li, Y. Yu, P. Zhou, H.J. Yan, Enhancement of boiling heat transfer using hydrophilic-hydrophobic mixed surfaces: a lattice Boltzmann study, Appl. Therm. Eng. 132 (2018) 490–499.
[13] X. Shan, H. Chen, Lattice Boltzmann model for simulating flows with multiple phases and components, Phys. Rev. E 47 (3) (1993) 1815–1819.
[14] L. Chen, Q. Kang, Y. Mu, Y.-L. He, W.-Q. Tao, A critical review of the pseudopotential multiphase lattice Boltzmann model: methods and applications, Int. J. Heat Mass Tran. 76 (2014) 210–236.
[15] S. Gong, P. Cheng, Lattice Boltzmann simulation of periodic bubble nucleation, growth and departure from a heated surface in pool boiling, Int. J. Heat Mass Tran. 64 (3) (2013) 122–132.
[16] S. Gong, P. Cheng, Lattice Boltzmann simulations for surface wettability effects in saturated pool boiling heat transfer, Int. J. Heat Mass Tran. 85 (2015) 635–646.
[17] Q. Li, Q.J. Kang, M.M. Francois, Y.L. He, K.H. Luo, Lattice Boltzmann modeling of boiling heat transfer: the boiling curve and the effects of wettability, Int. J. Heat Mass Tran. 85 (2015) 787–796.
[18] S. Gong, P. Cheng, Direct numerical simulations of pool boiling curves including heater's thermal responses and the effect of vapor phase's thermal conductivity, Int. Commun. Heat Mass Tran. 87 (2017) 61–71.
[19] W.Z. Fang, L. Chen, Q.J. Kang, W.Q. Tao, Lattice Boltzmann modeling of pool boiling with large liquid-gas density ratio, Int. J. Therm. Sci. 114 (2017) 172–183.
[20] X. Ma, P. Cheng, 3D simulations of pool boiling above smooth horizontal heated surfaces by a phase-change lattice Boltzmann method, Int. J. Heat Mass Tran. 131 (2019) 1095–1108.
[21] X. Ma, P. Cheng, X. Quan, Simulations of saturated boiling heat transfer on bio-inspired two-phase heat sinks by a phase-change lattice Boltzmann method, Int. J. Heat Mass Tran. 127 (2018) 1013–1024.
[22] Y. Yu, Z.X. Wen, Q. Li, P. Zhou, H.J. Yan, Boiling heat transfer on hydrophilic-hydrophobic mixed surfaces: a 3D lattice Boltzmann study, Appl. Therm. Eng. 142 (2018) 846–854.
[23] Q. Li, K.H. Luo, Achieving tunable surface tension in the pseudopotential lattice Boltzmann modeling of multiphase flows, Phys. Rev. E - Stat. Nonlinear Soft Matter Phys. 88 (5) (2013), 053307.
[24] Q. Li, J.Y. Huang, Q.J. Kang, On the temperature equation in a phase change pseudopotential lattice Boltzmann model, Int. J. Heat Mass Tran. 127 (2018) 1112–1113.
[25] L. Li, C. Chen, R. Mei, J.F. Klausner, Conjugate heat and mass transfer in the lattice Boltzmann equation method, Phys. Rev. 89 (4) (2014), 043308.
[26] P.J. Berenson, Film-boiling Heat Transfer from a Horizontal Surface, 1961.
[27] X. Quan, G. Chen, P. Cheng, A thermodynamic analysis for heterogeneous boiling nucleation on a superheated wall, Int. J. Heat Mass Tran. 54 (21) (2011) 4762–4769.